Heliyon 10 (2024) e27274

Contents lists available at ScienceDirect

Heliyon

journal homepage: www.cell.com/heliyon

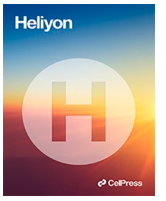

Research article

Spatiotemporal climate variability and trends in the Upper Gelana Watershed, northeastern highlands of Ethiopia

Sileshi Tadesse [a,b,*], Asnake Mekuriaw [a], Mohammed Assen [a]

[a] Department of Geography and Environmental Studies, Addis Ababa University, P.O.Box 1176, Addis Ababa, Ethiopia
[b] Department of Geography and Environmental Studies, Kotebe University of Education, P.O.Box 31248, Addis Ababa, Ethiopia

ARTICLE INFO

Keywords:
TAMSAT
CHIRPS
Rainfall
Temperature
Climate variability
Innovative trend analysis
Spatiotemporal trend analysis

ABSTRACT

The aim of this study was to evaluate the performance of CHIRPS and TAMSAT satellite rainfall data over the Upper Gelana watershed, where gauged meteorological data to understand the nature of the climate are scarce. In addition, variability and trends in rainfall and temperature were examined from 1983 to 2021. To evaluate satellite rainfall, categorical and continuous validation statistics were used. Trends were analyzed using Mann-Kendall, Sen's Slope estimator, and innovative trend analysis (ITA) methods. The study also utilized time-series geostatistical analysis techniques. The validation statistics show that TAMSAT performs better on the daily timescale, while the two products have comparable performance on the monthly timescale. TAMSAT was chosen for rainfall analysis because of its higher resolution and performance. The results reveal high inter-annual spatiotemporal variability and strong irregularities in monthly rainfall. The Mann-Kendall test indicates statistically significant positive trends in *kiremt* and annual rainfall, but *belg* rainfall exhibits an insignificant negative trend. In the *kiremt* season, we found a 96.1, 101.6, and 104.8 mm decadal rate of rainfall increment in the *lower weina dega* (LWD), *upper weina dega* (UWD), and *dega* agroecological zones, respectively. In contrast, *belg* season rainfall declined by 16.4, 16.2, and 14.0 mm per decade in the LWD, UWD, and *dega* agroecology zones, respectively. The pixel-wise trend analysis also revealed trends and magnitudes of monthly, seasonal, and annual rainfall that vary across the study area. In both LWD and UWD annual minimum and maximum temperatures, respectively, showed significant decreasing and increasing trends, but in *dega* agroecology the trends were insignificant. The findings of rainfall and temperature trends using the ITA method demonstrated its ability to discover some hidden trends that were not detected by the MK test.

1. Introduction

Climate change is a global problem that attracts the attention of governments, non-government organizations, and researchers all over the world [1]. It affects both humans and the earth's ecosystem. Extreme events such as drought, heat waves, sea level rise and flooding endanger human health [2,3], damage infrastructure [4], and cause biodiversity loss throughout the globe [5–7]. Though it is a global problem, the impacts vary from place to place with a more pronounced effect in developing countries [4].

Climate change is a serious threat to East Africa. The frequency of extreme events has been increasing at an alarming rate in the

* Corresponding author. Department of Geography and Environmental Studies, Addis Ababa University, P.O.Box 1176, Addis Ababa, Ethiopia.
E-mail address: sileshi2008@gmail.com (S. Tadesse).

https://doi.org/10.1016/j.heliyon.2024.e27274
Received 22 March 2023; Received in revised form 7 February 2024; Accepted 27 February 2024
Available online 28 February 2024

region [8,9]. The majority of East Africa's population relies on rainfed agriculture, making the region particularly vulnerable to the harmful effects of climate variability and change [10]. Climate change has impacted millions of people in East African countries over the last few decades [11–13].

Being located in the East African region, Ethiopia is among the most vulnerable countries to the impacts of climate change [14–16]. Every year, a large number of people are affected by the direct impacts of climate extremes [13,17–19]. Climate change is affecting rainfed agricultural practices and crop yield, which would in turn affect food security [11,20–23]. To lessen its effects, appropriate adaptation and mitigation measures should be implemented, which require adequate knowledge of local-level variability and trends in rainfall and temperature.

Many parts of Ethiopia receive rainfall in the *kiremt* (main) and *belg* (minor) seasons, which occur from June to September and February to May, respectively. Various studies have been conducted on rainfall variability in the country [20–22,24,25]. However, the findings on the seasonal rainfall patterns are inconsistent in one way or another. For instance Ref. [24], reported general declining and increasing trends of rainfall over Ethiopia in the *belg* and *kiremt* seasons, respectively. Contrary to this [22], analyzed rainfall for three decades in Ethiopia and found no significant trends in annual and seasonal rainfall amounts in Ethiopia. Disparities were also found in studies conducted at the regional level. A study conducted in the Amhara region of Ethiopia found a decreasing trend in *belg* rainfall and an increasing trend in *kiremt* season rainfall [26]. On the other hand, increasing trends of *belg* season rainfall were reported for the same region [27]. Similarly to the seasonal rainfall, the annual rainfall trends reported in previous studies are not uniform across the country. Among others [25,27], found an increasing trend in annual rainfall in the northwestern Ethiopian highlands and over the Amhara region, respectively. Another study in the southern parts of Ethiopia found a decreasing trend in annual rainfall amounts [28].

In the northeastern highlands of Ethiopia, where the present study area is located, a study over a century-long timescale found a significant decreasing trend in the *belg* season and annual rainfall amounts. Nevertheless, the decline in *kiremt* rainfall amount was not significant [20]. Similar results were reported by Ref. [21] in the Woleka river basin in the northeastern highlands of Ethiopia, where they found a general decline in annual, *kiremt*, and *belg* rainfall on almost the same temporal scale. Yet, the trends in *kiremt* rainfall amounts in Ref. [21] were *significant.* The same authors found an insignificant declining trend from metrological data analysis [21].

Generally, previous studies on climate variability and trends had discrepancies in their findings. According to Ref. [29], such discrepancies are a result of factors that include differences in the data sources, the statistical method used for data analysis, and the study period covered. Most of these studies rely on observed data with a large number of missed values or very low-resolution gridded data and a single method of trend analysis. They were also carried out at the regional or country level and provide a generalized picture for policymakers at the national level. Undeniably, the climatic conditions of Ethiopia vary within a short distance, both in time and

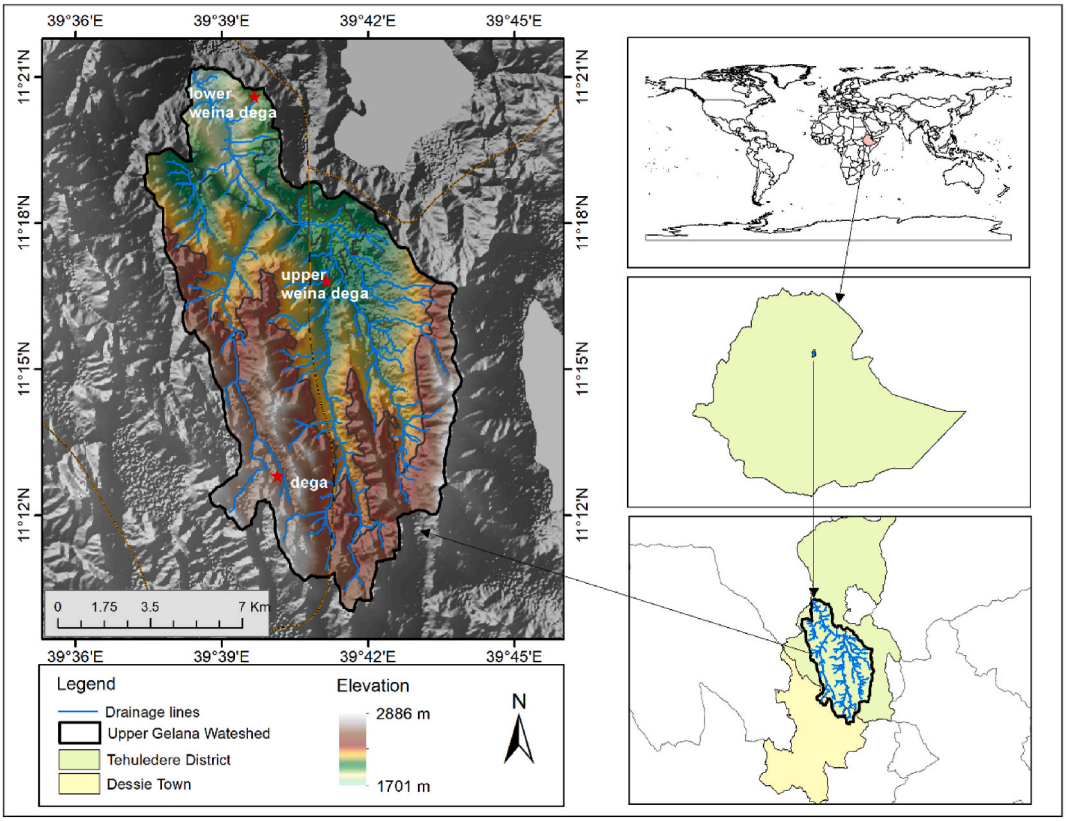

Fig. 1. Location map of the study area.

space. This demands a detailed investigation of local-level climate variability and change to help planners, decision-makers, and the local community develop and implement appropriate adaptation measures to reduce the impacts of climate variability and change. However, such studies are not available in the present study area, the Upper Gelana Watershed.

Therefore, this study was aimed at filling the gaps that existed in previous studies on climate variability and trends. First, to overcome the limitations pertinent to data, we examined the applications of high-resolution Earth Observation (EO) precipitation products, such as Tropical Applications of Meteorology using SATellite and ground-based observations (TAMSAT) and Climate Hazards Group Infrared Precipitation with Stations (CHIRPS), for local-level studies. The performance of satellite rainfall products varies based on topography, local climate, and the type of satellite [30–32]. As a result, we assessed their suitability at the watershed level using various statistical techniques. Second, we employed a pixel-wise geostatistical approach to the well-known Mann-Kendall (MK) test. In addition, the recently developed innovative trend analysis (ITA) was used to refine the findings of the MK test [33–39]. Moreover, variability and trends in rainfall and temperature were examined across the agroecological zones of the Upper Gelana watershed, in the northeastern highlands of Ethiopia.

2. Materials and methods

2.1. Description of the study area

The study was conducted in the Upper Gelana Watershed of Tehuledere district, in the northeastern highlands of Ethiopia. Geographically, it is found between 11.15^{o} N to 11.35^{o} N and 39.62^{o} E to 39.73^{o} E (Fig. 1). It covers a total area of 134 km^{2}. The study area is characterized by rugged topography. The altitude of the study area ranges from 1701 m to 2886 m above mean sea level. The upper part of the study area is occupied by mountains dissected by a series of smaller streams that flow to the Gelana mainstream.

The study area has *dega* (cool and humid) and *weina dega* (semi-humid) traditional agroecological zones based on altitude and rainfall, which are the primary criteria to classify the agroecology zones in Ethiopia [40,41]. *Dega* agroecology is located above 2300 m above sea level, while *weina dega* is located between 1701 and 2300 m above sea level; both receive rainfall ranging from 900 to 1400 mm. During our field observation, we have noted differences in plant and crop varieties grown in the lower and upper parts of the *weina dega* agroecology zone, mainly influenced by the climate conditions. To understand this distinction in climate conditions that exist within the *weina dega* agroecology zone of the study area, we have classified it into two equal parts based on the elevation: the lower *weina dega* (LWD) and upper *weina dega* (UWD) agroecology zones.

Major plant species found in the study area include planted *Eucalyptus* and naturally growing *Juniperus procera, Acacia abyssinica,* and *Euphorbia tirucalli.* A mixed traditional subsistence farming system consisting of both crop and animal production is the main source of livelihood in the study area. Major crops grown in the study area include *teff* (*Eragrostis tef*), wheat (*Triticum aestivum*), and sorghum (*Sorghum bicolor*) which are widely grown crops in the *dega* and *weina dega* zones. In addition to cereal crops, farmers produce *chat* (*Catha edulis*), a primary cash crop for the local community. The Upper Gelana watershed is among the most highly populated areas in Ethiopia, with limited cultivatable land in the South Wollo zone [42].

2.2. Data sources

In this study, satellite precipitation data is the principal data source for rainfall variability and trend analysis. Ground-based or observed rainfall data were used to assess the performance of satellite rainfall products. In order to examine the variability and trends in temperature, gridded temperature data were used. Supportive qualitative data about the variability and trend of rainfall were also acquired through focus group discussions (FGDs) and key informant interviews (KIIs).

2.2.1. Satellite preciptation data

Satellite precipitation data is vital to overcome the data scarcity caused by the limited spatial coverage of ground-based observations. Among the various available satellite precipitation products [43], two widely used satellite precipitation products, CHIRPS and TAMSAT version 3.1, were selected based on their long temporal coverage and relatively better spatial resolution.

CHIRPS is a satellite rainfall estimate derived from infrared Cold Cloud Duration (CCD) observations. It provides daily and monthly rainfall data from 1981 to the present with an average spatial resolution of 0.05° (5.5 km). This precipitation data is essential, particularly in sparsely gauged locations [44]. CHIRPS daily data [44] from 1983 to 2021 were retrieved from Google Earth Engine (GEE) Snippet ee.ImageCollection ("UCSB-CHG/CHIRPS/DAILY") using rgee, a package used to call GEE in the R environment [45].

TAMSAT is another satellite rainfall data source. The product is delivered by the TAMSAT group [46–48]. The data is derived from Meteosat thermal infrared (TIR) imagery using cold cloud duration (CCD). The TAMSAT has provided long-term rainfall data since 1983 with an average spatial resolution of 0.0375° (4 km) and temporal resolutions of daily, pentadal, dekadal, monthly, and seasonal time scales. The data in netCDF were retrieved from the TAMSAT website at http://www.tamsat.org.uk/data.

2.2.2. Observed rainfall data

Observed rainfall data from Haik station (found in the study area) as well as the Dessie, Ruga, and Kutaber stations found in the vicinity of the study area was obtained from the Ethiopian Meteorological Institute (EMI). The observed rainfall were used for validation of satellite precipitation data. To make a reliable comparison of the performances of satellite products across the stations, only precipitation records available on dates that are common to all four stations are considered, and missed values are disregarded. The location, elevation, and temporal coverage of stations used for satellite rainfall validation are presented in Table 1.

2.2.3. Gridded temperature data

We used gridded temperature data to examine the spatiotemporal variability and trends of temperature in the study area. The daily gridded temperature data with a spatial resolution of 0.0375° (4 km) over the study area were obtained from the EMI. Due to problems related to instruments and security issues that occurred in northern Ethiopia, including the study area, the metrological data for the Haik stations were not available in the last five years. Unfortunately, the gridded temperature from EMI is available only until 2018 for the whole of Ethiopia. As a result, we examined temperature from 1983 to 2018.

2.2.4. Interview and focus group discussion

To better understand farmers' perspectives on climate variability and change, three focus group discussions with five participants each were held in *lower weina dega (*LWD*), upper weina dega (*UWD*)* and *dega* agroecological zones. In addition, interviews were conducted with twelve key informants, four from each of the three agroecology zones, including community leaders, kebele heads, and agricultural extension workers. Participants for focus group discussions and key informant interviews were chosen based on their long-term residence in the area and familiarity with the issues under consideration.

2.3. Methods of data analysis

2.3.1. Validation methods

The performance of satellite precipitation is affected by several factors, including climate regimes, topography, and the type of satellite [30–32]. Thus, it is essential to evaluate the accuracy of CHIRPS and TAMSAT in the Upper *Gelan* watershed before using them for further analysis. Several categorical and continuous-verification statistical tools were used to assess performance on daily and monthly timescales.

Continuous verification statistics were used to quantify the level of accuracy, or how well the satellite estimates rainfall amounts as compared to the ground observations. The continuous verification statistics used in this study include the multiplicative bias, mean error (ME), mean absolute error (MAE), root mean square error (RMSE), Pearson Correlation Coefficient (r), and Nash–Sutcliffe Efficiency Coefficient (NSE). Bias and NSE were used to validate the daily and monthly satellite rainfall, respectively, while the other statistics were applied to both timescales.

The multiplicative bias is the comparison of the magnitude of the average satellite-estimated rainfall to that of the average rainfall from ground-based observations. The value of multiplicative bias ranges from negative infinity to positive infinity, with one being the perfect score [49].

$$\text{Bias (Multiplicative)} = \frac{\frac{1}{N}\sum_{i=1}^{N} Si}{\frac{1}{N}\sum_{i=1}^{N} Gi} \tag{1}$$

The mean error (ME) also called additive bias, measures the difference between the average satellite-estimated rainfall and the average ground observation [50,51]. Higher average satellite measurements than the gauged rainfall yield a positive ME value, while the reverse results in a negative ME value [51].

$$ME = \frac{1}{N}\sum_{i=1}^{N} (Si - Gi) \tag{2}$$

The Mean Absolute Error (MAE) measures the average magnitude of the errors between each pair of satellite-estimated and observed rainfall values. MAE values equal to zero imply that the satellite-estimated rainfall is accurate, and they rise as the differences between the estimated and observed rainfall become greater. It takes the same unit as the estimated rainfall [51].

$$MAE = \frac{1}{N}\sum_{i=1}^{N} |Si - Gi| \tag{3}$$

The RMSE also measures the average magnitude of the errors but gives greater weight to the larger errors [50]. It has the same scale as the satellite-estimated rainfall [51].

Table 1
List of meteorological stations used for validation and their locations based on the geographic coordinate system and Adindan datum.

No	Stations	Latitude	Longitude	Year	Elevation (m)
1	Ruga	11.17	39.58	1983–2007	2672
2	Dessie	11.12	39.63	1983–2007	2553
3	Haik	11.30	39.68	1983–2007	1985
4	Kutaber	11.27	39.53	1983–2007	1740

$$RMSE = \sqrt{\frac{1}{N}\sum_{i=1}^{N}(Si - Gi)^2} \tag{4}$$

The correlation coefficient (r) measures the degree of a linear relationship between the satellite-estimated rainfall and rain gauge data [50]. Its value ranges from +1 to −1, where the two upper and lower bounding values indicate a perfect linear relationship. If the value is zero, then it indicates no linear relationship [51].

$$\mathrm{r} = \sum \frac{(Si - \bar{S})\,(Gi - \bar{G})}{\sqrt{\sum (Si - \bar{S})^2}\sqrt{\sum (Gi - \bar{G})^2}} \tag{5}$$

Nash–Sutcliffe Efficiency (NSE) is a widely used index developed by Ref. [52] that measures the agreement between estimated and observed events. Its value ranges from minus infinity to one, where the latter indicates an excellent match between the estimated and observed event.

$$\mathrm{NSE} = 1 - \frac{\sum_{i=1}^{N}(Si - Gi)^2}{\sum_{i=1}^{N}(Gi - \overline{G})^2} \tag{6}$$

In all the above formulas for continuous validation statistics, S*i* represents the satellite-estimated value, G*i* is the observed rain gauge value, N is the number of observed samples, $\bar{}$G is the average observed rain gauge value, and $\bar{}$S is the average satellite-estimated value. In the case of Bias and NSE the variables refer daily and monthly satellite rainfall, respectively, whereas in the other continuous statistics variables refer to both timescales.

Categorical verification statistics were also used to assess the match between rainfall incidences in the satellite estimate and ground observations. Categorical verification statistics are calculated from two-by-two contingency tables of yes/no events with four basic elements such as hit, misses, false alarms, and correct negatives [50]. A hit (a) refers to a matched record of rainfall events in both the satellite estimate and ground-based observations. A false alarm (b) refers to a rainfall event recorded by satellite where there is no corresponding recorded rainfall by the ground-based meteorological stations in the study area at any time during the study period. A miss (c) refers to a rainfall event recorded by ground observation but missed in the satellite estimate. A correct negative (d) refers to no rainfall events in both satellite estimates and ground-based observations. In this study, we used categorical verification statistics such as the probability of detection (POD), false alarm ratio (FAR), threat score (TS), equitablethreat score (ETS), Heidke Skill Score (HSS), and frequency bias score to evaluate the daily satellite rainfall estimate. In computing these statistics, 0.1 mm was used as a threshold to separate the rain and non-rain events.

The probability of detection (POD) tells about the fraction of rain events recorded by the rain gauge, which was also correctly estimated by the satellite [50,51].

$$\mathrm{POD} = \frac{\mathrm{a}}{\mathrm{a} + \mathrm{c}} \tag{7}$$

The false alarm ratio (FAR) measures the fraction of rain events estimated by the satellite that did not happen in reality [50]. The best value for POD is one, and for FAR it is zero.

$$\mathrm{FAR} = \frac{\mathrm{b}}{\mathrm{a} + \mathrm{b}} \tag{8}$$

Heidke Skill Score (HSS) refers to the accuracy of the satellite rainfall estimate in relation to that of random chance. An HSS value of one indicates a perfect satellite estimate, and zero implies no skill. When the satellite rainfall products become worse than the reference data, the HSS value becomes negative [51].

$$\mathrm{HSS} = \frac{\mathrm{a} * \mathrm{d} - \mathrm{b} * \mathrm{c}}{(\mathrm{a} + \mathrm{c})(\mathrm{c} + \mathrm{d})(\mathrm{a} + \mathrm{b})\,(\mathrm{b} + \mathrm{d})} \tag{9}$$

The threat score (TS) is the number of correct yes forecasts divided by the total number of occasions on which that event was forecast and/or observed. Its value ranges between 0 and 1, where zero indicates a poor estimate and 1 is the perfect threat score [51].

$$\mathrm{TS} = \frac{\mathrm{a}}{\mathrm{a} + \mathrm{c} + \mathrm{b}} \tag{10}$$

The equitable threat score (ETS) is a modified version of the threat score (TS) that was developed to address the TS's flaw of being higher in wet areas. Its value ranges from 0 to 1, with 1 indicating perfect agreement between estimated and observed rainfall [50].

$$\mathrm{ETS} = \frac{\mathrm{a} - \mathrm{a}_{random}}{\mathrm{a} + \mathrm{c} + \mathrm{b} - \mathrm{a}_{random}} \tag{11}$$

The frequency bias score is a comparison of the frequency of rainfall in the satellite estimate to that of the observed rainfall [50]. It is a ratio of the total rain events in the satellite estimate to the total rain events observed. The bias value of one implies a perfect satellite rainfall estimate. Bias values larger than one signify a more frequent satellite rain estimate than a rain gauge record, whereas a

value less than one implies a less frequent rain event in the satellite estimate [51].

$$\text{Frequency bias} \,/\, \text{Bias score} = \frac{a+b}{a+c} \tag{12}$$

The continuous and categorical statistics were computed in R using the verification [53] and matrices [54] packages.

2.3.2. Methods for climate variability analysis

In this study, variability and trend analysis of rainfall and temperature were done on a pixel by pixel basis and at three point locations representing the LWD, UWD, and *dega* agroecological zones of the Upper Gelana watershed. The mean and standard deviation were used to examine the variability of rainfall and temperature in monthly, seasonal and annual time scale. These descriptive statistics are important to get an overview of rainfall and temperature variation during the study period. Apart from the mean and standard deviation, the coefficient of variation (CV), precipitation concentration index (PCI) and standardized rainfall anomaly (SRA) were analyzed.

2.3.2.1. Coefficient of variation (CV). The coefficient of variation is vital for understanding the degree of variability in rainfall from the long-term mean. The coefficient of variation was computed for monthly, seasonal, and annual timescales using the formula provided by [55].

$$CV = \frac{\sigma}{\overline{X}} * 100 \tag{13}$$

Where σ is the standard deviation and $\overline{X}$ is the long-term mean of preciptation data

2.3.2.2. Precipitation concentration index (PCI). To analyze the monthly rainfall distribution, the precipitation concentration index (PCI) was calculated using the formula given by Ref. [55].

$$PCI = 100\ \frac{\sum xi^{\,2}}{(\sum xi)^2} \tag{14}$$

Where *xi* is the rainfall amount of the *i*th month, and $\sum xi$ is the sum of precipitation for twelve months. PCI values less than 10 indicate uniform distribution, values between 10 and 15 represent moderate distribution, values from 15 to 20 show irregular distribution, and values above 20 indicate strong irregularity in precipitation distribution [55]. These classifications were used in previous studies [21,56,57].

2.3.2.3. Standardized rainfall anomaly (SRA). Standardized rainfall anomaly (SRA) is used to examine inter-annual rainfall variability and is specifically useful to identify wet and dry years. The standardized rainfall anomaly (SRA) for a given station can be calculated as used in Refs. [29,58,59].

$$SRA = \frac{Xt - \overline{X}}{\sigma} \tag{15}$$

Where *Xt* is the observed annual or seasonal rainfall in year t, $\overline{X}$ is the long-term mean annual or seasonal rainfall in the study period, and σ is the standard deviation of annual or seasonal rainfall. SRA values less than −1.65 indicate extreme drought; from −1.28 to −1.65, severe drought; −0.84 to - 1.28, moderate drought; and SRA greater than - 0.84, no drought [60]. SRA was used for analyzing rainfall variability in previous studies [29,58,59].

2.3.3. Trend analysis methods

2.3.3.1. Mann-Kendall (MK) trend test. Trends in timeseries climate data can be computed using parametric or non-parametric methods. In the case of the parametric method, the data must be independent and uniformly distributed, whereas non-parametric statistics do not consider distribution and can be used with non-serially correlated data. The Mann-Kendall test is one of the most commonly used non-parametric approaches for detecting statistically significant trends in rainfall and temperature [61,62]. To avoid drawing incorrect conclusions from the MK results, it is crucial to determine statistically significant autocorrelation in the data [63]. When there was no serial correlation, the Mann-Kendall test was utilized in this study to detect trends in the monthly, seasonal, and yearly rainfall and temperature [64–66]. The Mann-Kendall statistic S is given as:

$$s = \sum_{i=1}^{n-1} \sum_{j=i+1}^{n} sgn(x_j - x_i) \tag{16}$$

Where n is the number of data points, x_i and x_j are the data values in time series i and j (j > i), respectively, and sgn $(x_j - x_i)$ is the sign function as:

$$sgn(x_j - x_i) = \begin{cases} +1, if\ x_j - x_i > 0 \\ 0, if\ x_j - x_i = 0 \\ -1, if\ x_j - x_i < 0 \end{cases} \quad (17)$$

The variance is computed as:

$$Var(S) = \frac{n(n-1)(2n+5) - \sum_{i=1}^{m} t_i(i-1)(2ti+5)}{18} \quad (18)$$

Where n is the number of observations, m is the number of tied groups, and t_i denotes the number of ties of extent i. A tied group is a set of sample data with the same value. In cases where the sample size $n > 10$, the standard normal test statistic Z_S can be calculated as follows:

$$Z_s = \begin{cases} \frac{S-1}{\sqrt{Var(S)}}, if\ S > 0 \\ 0 \quad if \quad S = 0 \\ \frac{S+1}{\sqrt{Var(S)}}, if\ S < 0 \end{cases} \quad (19)$$

Positive values of Z_S indicate increasing trends, while negative Z_S values show decreasing trends.

In this study, the presence of serial-autocorrelation was assessed using the autocorrelation function (acf) of the stat package in the R program [67]. In the presence of significant serial-correlation, pre-whitening was applied following the variance correction approach to address serial correlation in trend analysis [68]. The pre-whitening procedure was implemented using the modifiedmk package in R [69].

2.3.3.2. Sen's slope estimator. Sen's slope estimator was used to quantify the magnitude of detected trends. It is calculated using the formula given as follows [64].

$$X_{ij} = \frac{(Y_j - Y_i)}{t_j - t_i} for\ \ i = 1, \ldots, N \quad (20)$$

Where the X_{ij} are the slopes of the lines connecting each pair of points (t_i, Y_i) and (t_j, (Y_j) where ($t_j > t_i$. A positive value of X_{ij} indicates an increasing trend, while a negative value of X_{ij} indicates a decreasing trend [70].

For better visualization of results from coarse resolution rainfall analysis, values from each pixel were extracted and interpolated back using inverse distance weighted (IDW) interpolation using the spatstat package [71]. Then, ArcGIS 10.7.1 and Origin 2022 were used to prepare the figures.

2.3.3.3. Innovative trend analysis (ITA). The ITA is graphical approach for analyzing trends in time series data, first developed by Ref. [39]. Non-parametric trend analysis techniques like the Mann-Kendall test need a timeseries data that are not serially correlated. However, the ITA completely avoids such prior assumptions based on the data [33,35,39,72]. In this method, the data is divided into two equal parts and then plotted on a scatter plot, with the first half on the horizontal axis and the second half on the vertical axis. Data points below the 1:1 (45°) line show a decreasing trend, whereas data points above the 1:1 (45°) line show an increasing trend. Points that fall on the 45° line are considered trendless. The ITA graph can also be interpreted by dividing the data point series into three equal clusters based on the minimum and maximum value ranges of the data points on the horizontal axis. Then, the three clusters can be labeled as "low," "medium," and high," and interpretations of the trends can be provided for each cluster. The significance of the trend can be determined using ±5 % or ±10% error. If the data points are outside of ±5 % error or the maximum ±10% error from the 1:1 line, the trend is significant [72]. We used the ITA method to refine the findings of the Mann-Kendall trend analysis [33–36,73,74].

Table 2
Continuous and categorical validation statistics for CHIRPS and TAMSAT daily rainfall in the upper Gelana watershed and its surroundings (the unit for ME, MAE and RMSE is mm).

Stations		Bias	ME	MAE	RMSE	r	POD	TS	ETS	FAR	HSS	Bias score
Ruga	CHIRPS	1.16	0.45	3.75	9.06	0.38	0.4	0.33	0.22	0.38	0.36	0.68
	TAMSAT	1.06	0.16	2.97	7.03	0.5	0.57	0.48	0.36	0.3	0.53	0.86
Haik	CHIRPS	0.86	−0.48	3.84	9.03	0.4	0.4	0.33	0.22	0.37	0.35	0.65
	TAMSAT	0.76	−0.84	3.15	7.55	0.51	0.56	0.47	0.35	0.29	0.52	0.82
Dessie	CHIRPS	0.91	−0.31	4.01	9.77	0.42	0.41	0.32	0.21	0.4	0.35	0.69
	TAMSAT	0.84	−0.57	3.33	8.2	0.52	0.59	0.47	0.35	0.32	0.52	0.88
Kutaber	CHIRPS	1	0.01	3.79	9.24	0.43	0.41	0.33	0.22	0.37	0.37	0.67
	TAMSAT	0.89	−0.36	2.87	6.9	0.59	0.6	0.51	0.4	0.26	0.57	0.84

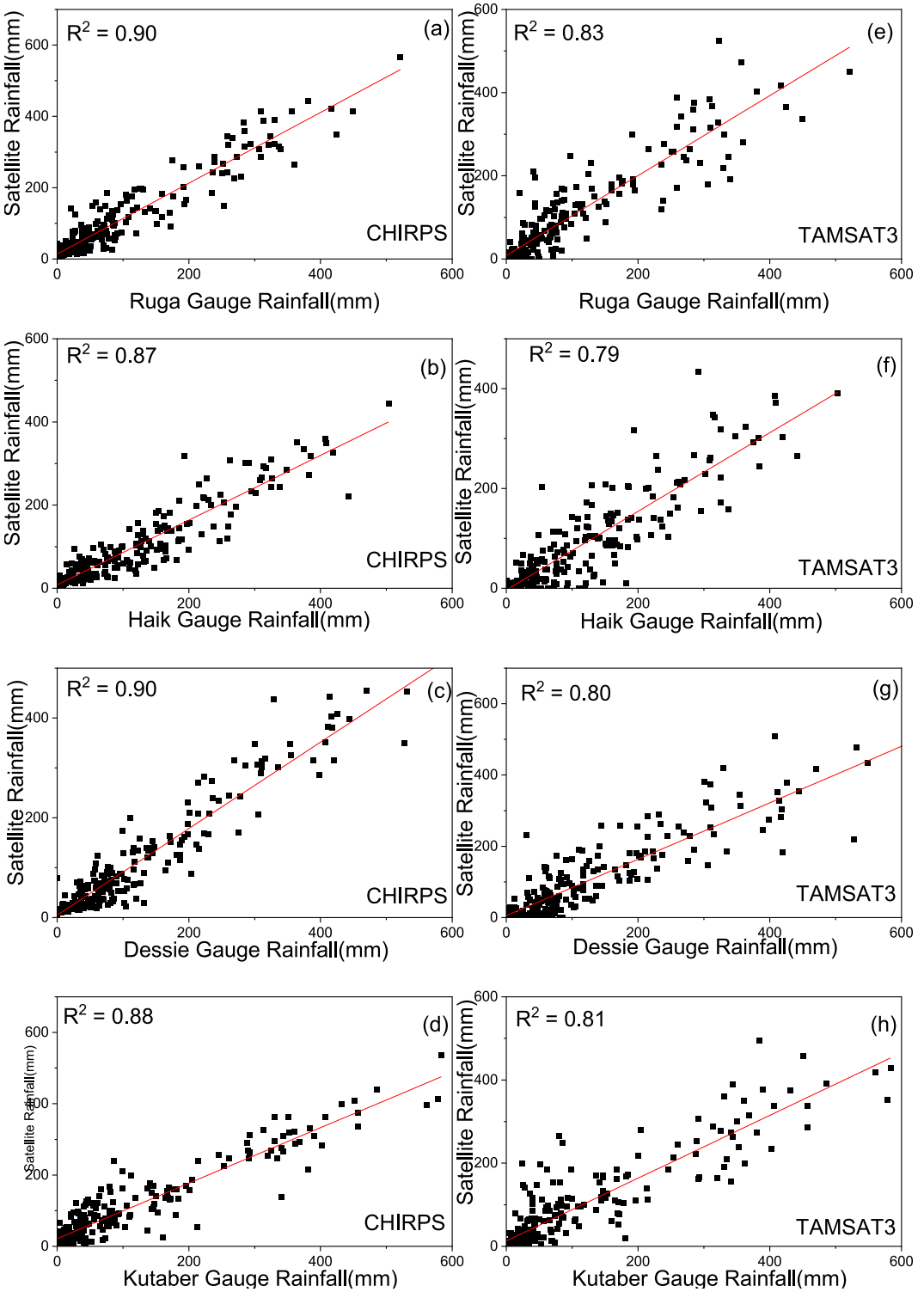

Fig. 2. The relationship between CHIRPS (a–d) and TAMSAT (e–h) monthly rainfalls and rain gauge data at Ruga, Haik, Dessie and Kutaber stations that are found in the upper Gelana watershed and its surroundings.

3. Results and discussions

3.1. Evaluation of CHIRPS and TAMSAT satellite rainfall

This section presents and discusses the validation results for the daily and monthly performances of CHIRPS and TAMSAT satellite rainfall.

3.1.1. Validation of CHIRPS and TAMSAT daily rainfall

For the daily timescale, the multiplicative bias statistics revealed that both satellite products are comparable to station rainfall in terms of average magnitude (Table 2). The multiplicative bias for TAMSAT ranges from 0.8 (Haik station) to 1.1 (Ruga station), and for CHIRPS it ranges from 0.9 (Haik station) to 1.2 (Ruga station). At Kutaber stations, CHIRPs have a perfect multiplicative bias score of 1.0. The MAE value for TAMSAT varies from 2.97 mm (Kutaber station) to 3.33 mm (Dessie station), while the MAE value for CHIRPS ranges from 3.75 mm (Ruga station) to 4.01 mm rainfall (Dessie station). The result of the MAE indicates that TAMSAT has better performance than CHIRPS. The RMSE value for TAMSAT ranges from 6.90 mm to 8.20 mm of rainfall, and for CHIRPS, it ranges from 9.03 mm to 9.77 mm of rainfall. This implies that TAMSAT has a lower average magnitude of error than CHIRPS. As compared with CHIRPS, the daily TAMSAT rainfall has a good linear correlation (r) with the rainfall values at the four meteorological stations. The POD value of CHIRPS at the four stations ranges from 0.40 to 041, and for TAMSAT, it ranges from 0.56 to 0.60 (Table 2). This indicates TAMSAT has better performance in detecting daily rain events in the Upper Gelana watershed and its vicinity. The findings of this study agree with the comparison of the two products in terms of POD in the northwest part of the Rift Valley in Ethiopia [31].

The TS and ETS statistics showed that CHIRPS have almost consistent performances over the four stations, while the performance of TAMSAT was more or less the same except for the Kutaber station (Table 2). In comparison, TAMSAT has higher TS and ETS values than CHIRPS, implying a better ability to detect rain events. The FAR values for TAMSAT are lower than CHIRPS at all stations, suggesting that TAMSAT produces fewer false alarms. This also implies that the rain events that did not occur in reality were reported as if they did by TAMSAT were smaller than those in CHIRPS. The HSS result, which measures the skill or accuracy of satellite precipitation in relation to random chances, showed that TAMSAT has better accuracy than CHIRPS for daily rainfall. Similar findings with the HSS result of this study were also reported by Ref. [31]. The comparison bias score revealed that the frequencies of TAMSAT are more similar to the frequencies of station rainfall than those of CHIRPS (Table 2). In general, almost all of the continuous and categorical statistics show that TAMSAT performs better than CHIRPS in the daily rainfall estimates. Similar findings were reported by Ref. [31] who attributed the better performance of the TAMSAT daily rainfall product to the inherent algorithm adjusted based on local station data.

3.1.2. Validation of CHIRPS and TAMSAT monthly rainfall

The patterns in the scatterplots and the coefficient of determination (R^2) values show a significant correspondence between the monthly rainfall from satellite products and the observed rainfall patterns at all four stations (Fig. 2). However, both the scatter and values of (R^2) suggest that the monthly rainfall from CHIRPS (Fig. 2a–d) has slightly better accuracy than monthly rainfall from TAMSAT (Fig. 2e–h). Similar pattern of scatters for both CHIRPS (less) and TAMSAT (a bit wider) over Ethiopia were reported in Ref. [31].

As shown in Table 3, the mean error at Ruga is 13.49 mm and 4.97 mm for CHIRPS and TAMSAT, respectively. The result indicates that TAMSAT has a lower average error compared to CHIRPS at Ruga station. It also shows that the rainfall measured by the CHIRPS satellite is greater than the rainfall measured at the Ruga meteorological station. The mean error for CHIRPS at Haik, Dessie, and Kutaber stations, respectively, is −14.6 mm, −9.5 mm, and 0.15 mm. While the mean error for TAMSAT at Haik, Dessie, and Kutaber stations is −25.3 mm, −17.1 mm, and −10.8 mm, respectively (Table 3). The findings imply that CHIRPS has a lower average error than TAMSAT at the three stations. The negative mean error values for both CHIRPS and TAMSAT suggest that the estimated rainfall by these satellite products is lower than the rainfall measured at the respective ground-based meteorological stations. For CHIRPS, the MAE values range from 25.5 mm at Dessie to 31.3 mm at Kutaber station, while TAMSAT MAE values range from 28.5 mm at Ruga to 38.9 mm at Dessie station (Table 3). Similar to ME, the MAE and the RMSE statistics revealed that CHIRPS is slightly better than TAMSAT in monthly rainfall estimates at all four stations. The correlation coefficient for both CHIRPS and TAMSAT monthly satellite-estimated rainfall products is larger than +0.8, which demonstrates a very strong positive association with the observed rainfall. Both

Table 3
Validation statistics for CHIRPS and TAMSAT monthly rainfall in the upper Gelana watershed and its surroundings (the unit for ME, MAE and RMSE is mm).

Stations		ME	MAE	RMSE	*R*	NSE
Ruga	CHIRPS	13.49	25.58	36.28	0.95	0.88
	TAMSAT	4.97	28.35	45.20	0.92	0.82
Haik	CHIRPS	−14.63	29.31	42.19	0.93	0.84
	TAMSAT	−25.33	37.10	54.18	0.89	0.74
Dessie	CHIRPS	−9.46	25.54	39.39	0.95	0.90
	TAMSAT	−17.12	38.43	57.69	0.90	0.78
Kutaber	CHIRPS	0.15	31.29	46.04	0.94	0.87
	TAMSAT	−10.75	35.94	57.30	0.90	0.80

CHIRPS and TAMSAT have NSE values close to one, indicating very good agreement with observed rainfall at all stations. In general, all continuous statistical tests performed on monthly data from TAMSAT and CHIRPS indicate that the two products perform well, with CHIRPS slightly outperforming the TAMSAT satellite rainfall estimate. The results of this study, specifically MAE, correlation coefficient (r), and efficiency, are in line with the findings stated by Ref. [31] for the monthly timescale in Ethiopia.

3.2. Spatiotemporal variability of rainfall

3.2.1. Variability of monthly rainfall

Based on the validation results of satellite rainfall products, TAMSAT was better than CHIRPS for daily rainfall, while they had a very close performance on monthly rainfall. As a result, TAMSAT was chosen and, hence, used in the subsequent analyses of the variability and trend in rainfall in this study. As presented in Table 4, the mean monthly rainfall is high in August amounts to 268 mm, 270.9 mm, and 289.9 mm in LWD, UWD, and *dega* agroecology zones, respectively. Whereas January is the month with lowest mean monthly rainfall in all three agroecology zones. When comparing the three agroecology zones, *dega* received the highest mean monthly rainfall, followed by UWD and LWD, in the majority of the months. In the study area, the mean seasonal rainfall was high in the *kiremt* season (the main rainy season) and low in the *bega* season during the study period (1983–2021). The *belg* rainfall deviate from the mean by 96.8, 94.1 and 93.8 mm in LWD, UWD and *dega* agroecology zones, respectively. The standard deviation of annual rainfall is low (193.7 mm) and high (212.4 mm) in LWD and *dega*, respectively. The coefficient of variation (CV) was higher for the *belg* season than the *kiremt* and annual rainfall in all the three agroecology zones, indicating high variability.

The average monthly rainfall in the study area varies spatially and temporally across latitudes (north-south) and longitudes (east-west). The spatial variation could be related to the altitude of the study area. As we move north, the altitude drops and the agroecology shift from *dega* to UWD and eventually to LWD. It increases from east to west in the northern half, but the topography is uneven in the southern half. As shown in the Hovmoller diagrams in Fig. 3a, the southern parts (*dega*) of the study area received relatively high mean monthly rainfall in June, July, August, and September. As we moved north (LWD), the mean rainfall was high only in the July and August months. Similarly, the distribution of rainfall varies from east to west; places in the eastern part received relatively the highest mean monthly rainfall (1983–2021) in all of the *kiremt* months, but western parts do in July and August (Fig. 3b). Furthermore, as illustrated in Fig. 4a-l, the mean monthly rainfall has a distinct spatial pattern that is also related to the seasons.

3.2.1.1. Preciptation concentration index (PCI). Based on the PCI results, the LWD, UWD, and *dega* agroecology zones of the upper Gelana watershed are characterized by moderate to strong irregularities in rainfall distribution (Fig. 5a–c). The proportion of years with a moderate rainfall distribution is 2.6% in the LWD agroecology zone and 5% in the UWD and *dega* agroecology zones. The years 1997 and 2019 exhibited moderate rainfall distributions in the UWD and *dega* agroecology zones, as did the year 2019 in the LWD (Fig. 5). Additionally, 53.8% of study years in the LWD and UWD and 64% of the study years in *dega* had PCI values above 20, indicating a strong irregularity in the distribution of rainfall. As seen in Fig. 5a-c, the distribution of monthly rainfall was not uniform or homogeneous throughout the study periods (1983–2021).

3.2.2. Variability of seasonally and annual rainfall

As depicted in Fig. 8a-d, the distribution of the seasonal and annual mean rainfall follows a similar pattern as the mean monthly rainfall presented in Fig. 4a-l. The southern parts of the Upper Gelana watershed received relatively the highest mean *kiremt* season rainfall (740 mm), while the northern part of the watershed received relatively low (616 mm) mean *kiremt* season rainfall. As in the

Table 4
Descriptive statistics of the monthly, seasonal, and annual rainfall (unit of measurement is mm) based TAMSAT in the LWD, UWD and *dega* agroecology zones of the upper Gelana watershed (1983–2021).

Month	LWD			UWD			*Dega*		
	Mean	SD	CV	Mean	SD	CV	Mean	SD	CV
Jan	1.7	4.0	240.0	0.7	2.6	347.1	0.3	1.5	605.4
Feb	9.8	16.3	166.3	8.6	13.8	160.6	7.8	12.5	160.7
Mar	70.1	51.7	73.7	70.0	51.5	73.7	71.5	49.0	68.6
Apr	108.3	56.0	51.7	109.8	55.5	50.5	112.4	59.1	52.6
May	61.9	48.8	78.9	66.2	52.5	79.3	70.6	56.4	79.8
Jun	26.7	28.2	105.5	30.3	30.8	101.3	31.1	32.1	103.2
Jul	238.0	102.3	43.0	243.9	103.8	42.6	264.6	111.5	42.1
Aug	268.6	92.0	34.3	270.9	93.6	34.6	289.9	97.6	33.7
Sep	108.8	40.8	37.5	111.9	43.6	39.0	123.9	49.0	39.5
Oct	45.1	47.4	105.0	45.7	47.6	104.1	46.2	49.8	107.8
Nov	17.5	29.9	171.0	17.8	30.5	170.8	19.6	29.5	150.9
Dec	7.4	12.2	166.1	7.0	11.4	162.7	7.2	13.5	186.5
Season									
Belg (FMAM)	250.0	96.8	38.7	254.5	94.1	37.0	262.3	93.8	35.8
Kiremt (JJAS)	642.1	191.3	29.8	657.1	197.7	30.1	709.5	208.7	29.4
Bega(ONDJ)	72.0	53.9	74.9	71.7	55.7	77.8	73.3	59.4	81.0
Annual	963.8	193.7	20.1	982.9	200.7	20.4	1045.1	212.4	20.3

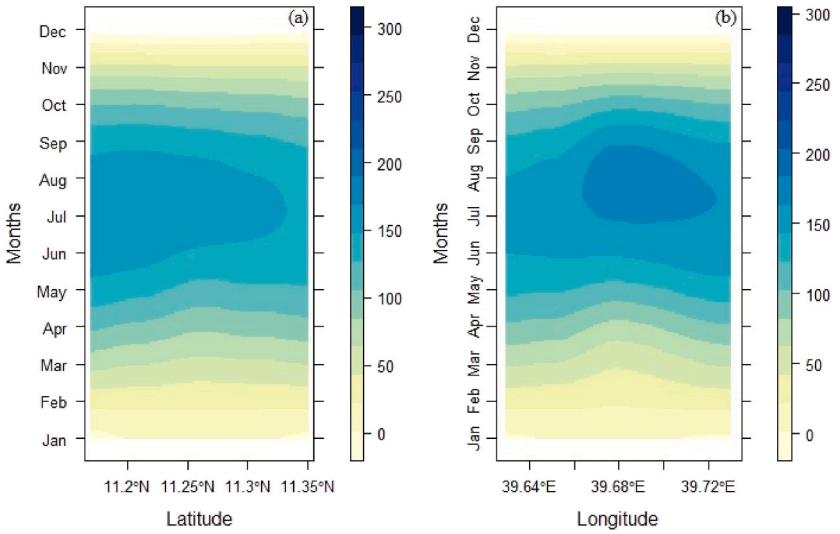

Fig. 3. Hovmoller diagrams prepared using TAMSAT data that show latitudinal (a) and longitudinal (b) variations of mean monthly rainfall (mm) in the Upper Gelana watershed (1983–2021).

mean monthly and seasonal rainfall, latitudinal and longitudinal variations were also visible in the annual rainfall time series (Fig. 6a and b). The annual rainfall decreased as we moved from east to west (Fig. 6b) and south to north (Fig. 6a), and the patterns were consistent throughout the study period (1983–2021). As stated above, the high rainfall in the southern and eastern parts may be associated with their high altitude and better forest cover than the northern parts.

3.2.2.1. Standardized rainfall anomaly (SRA). The analysis of seasonal SRA from 1983 to 2021 shows that the LWD agroecology zone experienced moderate and above drought conditions in 17.9% and 20.5% of the *belg* and *kiremt* seasons, respectively. In the UWD agroecology, 15.4% of the *belg* season and 20.5% of the *kiremt* season out of the 39 years were characterized by above-moderate drought conditions. During the study period, the proportion of dry years in the *dega* agroecology zone accounts for 15.4% and 17.9% during the *belg* and *kiremt* seasons, respectively. In all three agroecology zones, the years 1996 and 1999 were the wettest and driest of the *belg* season, respectively (Fig. 7a–c). The wettest *kiremt* season in the LWD and UWD occurred in 2010, but in the *dega* agroecology zone, it was in 1998. In all the agroecological zones, the driest *kiremt* season was recorded in the year 1984 (Fig. 7d–f). According to the annual SRA statistics, both the LWD and *dega* had moderate to extreme dryness in 20.5% of the study years; the UWD agroecology, however, saw slightly more dryness (23.1%). In terms of annual rainfall, 1984 and 2019 were the driest and wettest years common to all three agroecological zones, respectively (Fig. 7j-l). The standardized rainfall anomaly index results indicate that the study area has high inter-annual variability in seasonal and annual rainfall (Fig. 7a-l).

3.3. Spatiotemporal trends in rainfall

3.3.1. Serial-autocorrelation test

In order to get a proper result from the Mann-Kendall trend test, it is essential to assess the presence of serial autocorrelation. Thus, the lag-1 serial correlation was calculated on a pixel-by-pixel basis for monthly, seasonal, and annual rainfall. Significant autocorrelation ($P = 0.05$) was found in the January (Fig. 9a) and April (Fig. 9b) months on a few pixels. So, pre-whitening was applied for those pixels with significant autocorrelation following the variance correction approach to address serial correlation in trend analysis in R [68]. The pixels where the point values for LWD, UWD, and *dega* agroecology zones were extracted are not serially correlated. Fig. 9 shows the spatial autocorrelation for rainfall in January and April months.

3.3.2. Monthly rainfall Mann-Kendall trend analysis

As shown in Table 5, the monthly rainfall in the LWD agroecology showed statistically significant increasing trends in June ($P = 0.1$) and from July to November ($P = 0.05$). Similarly, the monthly rainfall in the UWD and *dega* agroecology zones shows a significant increasing trend from June to November. As.

shown in Table 5, Sen's slope test result indicates that the highest magnitude of the trend for all the agroecology zones was in August. In contrast, the MK test indicates statistically non-significant downward trends in the January to April, and December months in all three agroecology zones (Table 5). However, Sen's slope values for January, February, and December months were nearly zero, implying that the magnitude of changes in rainfall in these months were insignificant during the study period (1983–2021).

Fig. 10a-l and (a'-l'), respectively, shows the spatial patterns of Mann-Kendall and Sen's slope test statistics of monthly rainfall for the study period (1983–2021).The pixel-wise analysis showed the spatial variation in the magnitudes and significance levels of trends

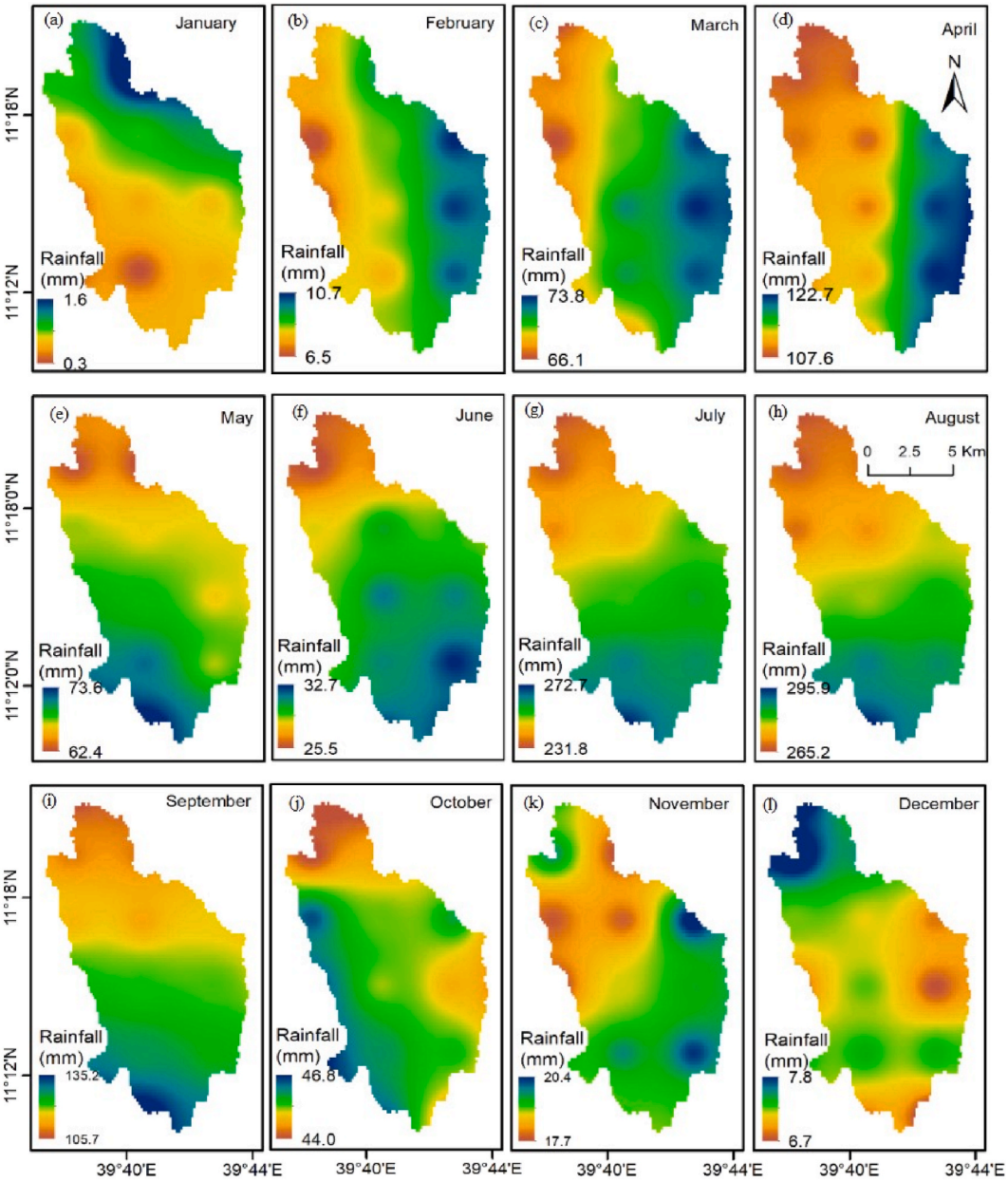

Fig. 4. Spatial distribution of mean monthly rainfall (mm) in the Upper Gelana Watershed (1983–2021) from January to December respectively labeled by letters a-l prepared based on TAMSAT data.

across the Upper Gelana watershed. For the majority of the months, the pixel-by-pixel trend analysis results are closely related to MK and Sen's slope results presented in Table 5. The exceptions were the trends in the March and May months. From the spatial analysis, a statistically significant (P = 0.1) decreasing trend was found in March in the north, northwest, and a small area in the southeast part of the watershed (Fig. 10c'). Contrary to MK and Sen's slope result for the monthly rainfall presented in Table 5, the spatial analysis shows an insignificant positive trend in May in the eastern part and negative trends in the western part (Fig. 10e').

3.3.3. Mann-Kendall trend analysis for seasonal and annual rainfall

Based on the pixel-wise trends shown in Fig. 11(d,d',dd), statistically significant increasing trends were found in the annual rainfall for the whole Upper Gelana watershed (P = 0.001). This result is in line with the findings of previous studies [29,75,76]. An increasing trend in annual rainfall were found for Dessie station in earlier study [29]. The magnitudes of the trend in annual rainfall vary spatially from 8.98 to 10.22 mm/year. It was lower in the northern part (LWD agroecology) and higher in most parts of UWD and *dega* agroecology zones of the study area. *Kiremt* season rainfall also shows a statistically significant (P = 0.001) positive trend (Fig. 11b,b',

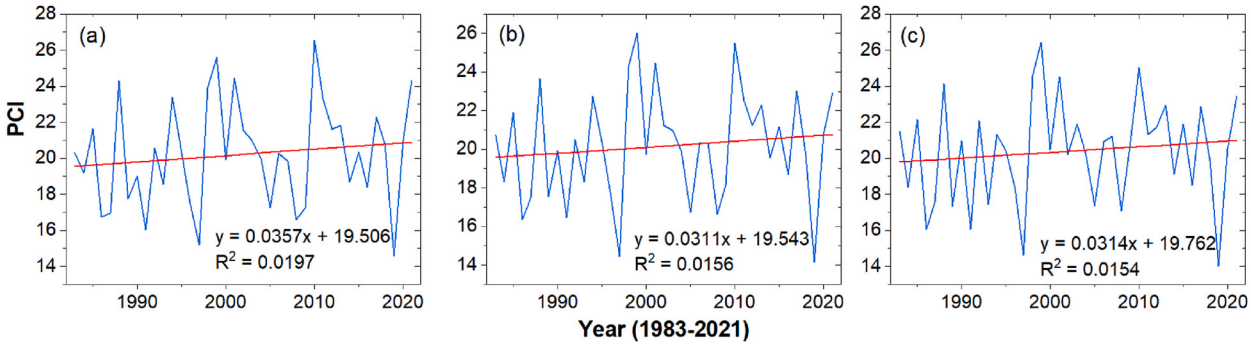

Fig. 5. PCI calculated from TAMSAT rainfall for LWD (a), UWD (b), and *dega* (c) agroecology zones of the Upper Gelana Watershed (1983–2021).

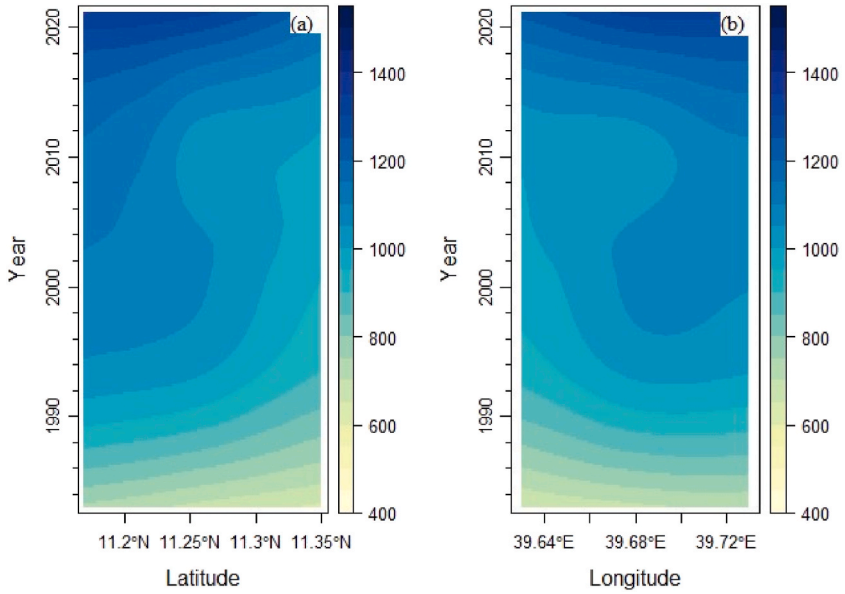

Fig. 6. Hovmoller diagrams prepared using TAMSAT data that show latitudinal (a) and longitudinal (b) variations of annual rainfall (mm) in the Upper Gelana watershed (1983–2021).

bb). Similar findings were reported by other researchers [29,75–79]. The annual increment of *kiremt* rainfall varies across the watershed from 9.38 mm (northern) to 11.4 mm (southern). Fig. 11(a,a',aa) also shows a declining trend in *belg* season rainfall throughout the study area, but it is insignificant. The decline in *belg* season rainfall was relatively high in the southern part (*dega*) of the Upper Gelana watershed. Similar findings on the decreasing trend in *belg* season rainfall were identified in previous studies [75,76,78,79]. In all agroecology zones of Upper Gelana watershed, the pattern of *bega* season rainfall shows a slight increment from 1983 to 2021 that is significant at $P = 0.05$ (Fig. 11c,c'cc).

In all agroecological zones of the study area, the annual, *bega*, and *kiremt* season rainfall showed a significant increasing trend, whereas *belg* season rainfall exhibits a non-significant decreasing trend (Fig. 12a-l). As determined from the Sen's slope in Fig. 12j-l, rate of increment in annual rainfall in the LWD, UWD and *dega* agroecology zones was 91.0, 94.4, and 99.0 mm per decade, respectively. Similarly, the decadal rate of increment of rainfall during *kiremt* season was 96.1, 101.6, and 104.8 mm in the LWD, UWD and *dega* agroecological zones the order of sequence computed based on Fig. 12d-f. In contrast, the *belg* season rainfall in the LWD, UWD and *dega* agroecology zones decreased by 16.4, 16.2, and 14.0 mm per decade, respectively. The findings imply that the decadal rate of increase in annual and *kiremt* season rainfall is higher in the *dega* agroecology zone and lower in the LWD.

3.3.4. Innovative trend analysis (ITA) of seasonal and annual rainfall

The ITA results in Fig. 13a-l were interpreted for the "low," "medium," and "high" clusters, as explained earlier. Accordingly, data points in the *belg* except for *dega* (Fig. 13a–c) and *bega* season (Fig. 13g–i) are below 1:1 (45°) line, indicating the decreasing trend of rainfall in these seasons. In contrast, the data points series of the *kiremt* season except *dega* (Fig. 13d–f) and annual rainfall (Fig. 13j-l) are above the 1:1 (45°) line, suggesting an overall increasing trend in rainfall.

The cluster-based interpretations of the ITA results in Fig. 13a-i revealed that the trends vary in the low, medium and high clusters

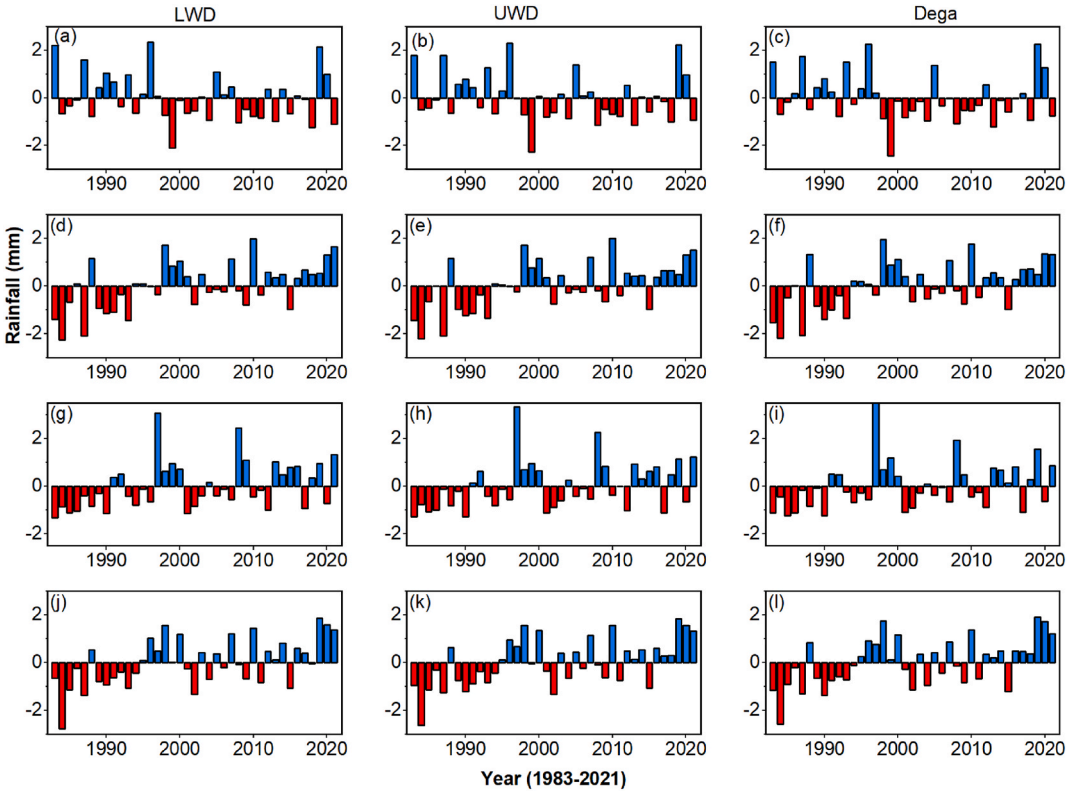

Fig. 7. The standardized anomaly index for the *belg* (a–c), *kiremt* (d–f), *bega* (g–i) and annual (j–l) in the LWD (first column), UWD (second column) and *dega* (third column) agroecology zone prepared using TAMSAT preciptation (1983–2021).

for seasonal rainfall. In LWD and UWD agroecology zones, a decreasing trend of *belg* season rainfall were identified in all three clusters of data points. However, the *belg* season in the *dega* agroecology showed an increasing, decreasing and no-trends in the low, medium and high clusters respectively. *Kiremt* season rainfall exhibited an increasing trend in the low, medium, and high data points in all three agroecology zones, with the exception of the decreasing trend in the high data points in *dega* agroecology. In the case of *bega* season, an increasing trend were detected in low and medium clusters, but rainfall showed a decreasing trends in the high cluster in all the agroecology zones of the study area (Table 6). As presented in Table 6 and Fig. 13j–l, the ITA show that the annual rainfall exhibits an increasing trend in low, medium, and high data point clusters in all the study agroecology zones.

3.3.5. Comparison of MK and ITA results for seasonal and annual rainfall

We found almost similar findings from MK and ITA methods in the overall trend directions for *belg, kiremt* and annual rainfall LWD and UWD agroecological zones of the study area. However, we found a contrasting findings in the *belg* and *kiremt* season rainfall in the *dega* agroecology. In this agroecology zone, the MK test show insignificant decreasing trend in *belg* rainfall, but the ITA revealed significant increasing trend in the low cluster and no-trend in the high cluster of the *belg* season rainfall. Likewise, we found a significant increasing trend of *kiremt* season rainfall from MK test, while ITA show significant declining trend in the high data point clusters. Similar contrasting results were obtained for *bega* season rainfall (Fig. 12 and Table 6). Other authors also noted similar discrepancies between the findings of MK and ITA [35]. This might be viewed as an advantage of ITA method in providing detailed results about trends in hydro-climatological timeseries data.

3.4. Spatiotemporal variability of temperature

In the upper Gelana watershed, the temperature is spatially variable (Fig. 14a–c). It is higher in the north (LWD) than the southern (*dega*) part. The lowest mean monthly maximum temperature were 24.1 °C, 23.5 °C, and 20.3 °C in the LWD, UWD, and *dega* agroecology zones, respectively, recorded in January. Whereas, the highest mean monthly maximum temperature were 30.3 °C, 29.6 °C, and 25.9 °C in June, in order of sequence, in the LWD, UWD, and *dega* agroecology zones. The lowest mean monthly minimum temperature is 7.3 °C (in LWD), 6.8 °C (in UWD), and 6.1 °C (*dega*) — observed in December. In contrast, the mean monthly minimum temperature were high in July in the LWD (14.1 °C), UWD (13.6 °C) and *dega* (11.9 °C) agroecological zones. The watershed experienced the highest seasonal average maximum and the lowest seasonal average minimum temperature in the *kiremt* and *bega* seasons, respectively (Table 7). The annual average maximum temperatures of the watershed were 26.6 °C, 26.0 °C, and 22.6 °C, in order of

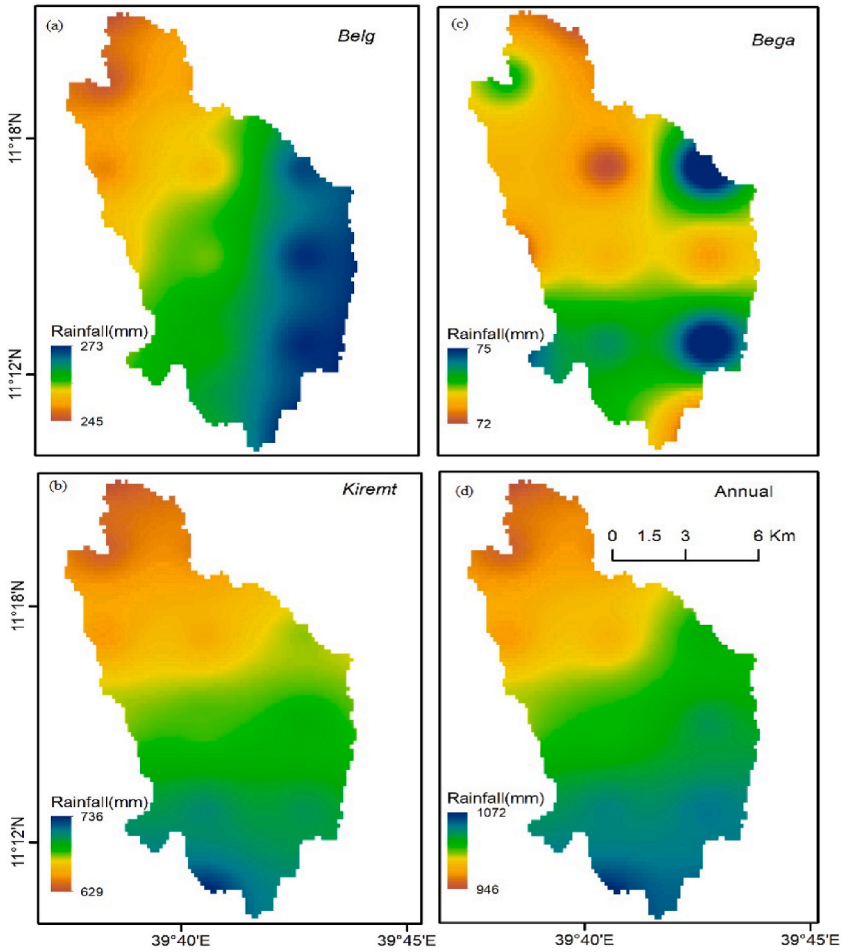

Fig. 8. Spatial distribution of average rainfall (1983–2021) in *belg* (a), *kiremt* (b) and *bega* (c) seasons and annual (d) timescales prepared based on TAMSAT data.

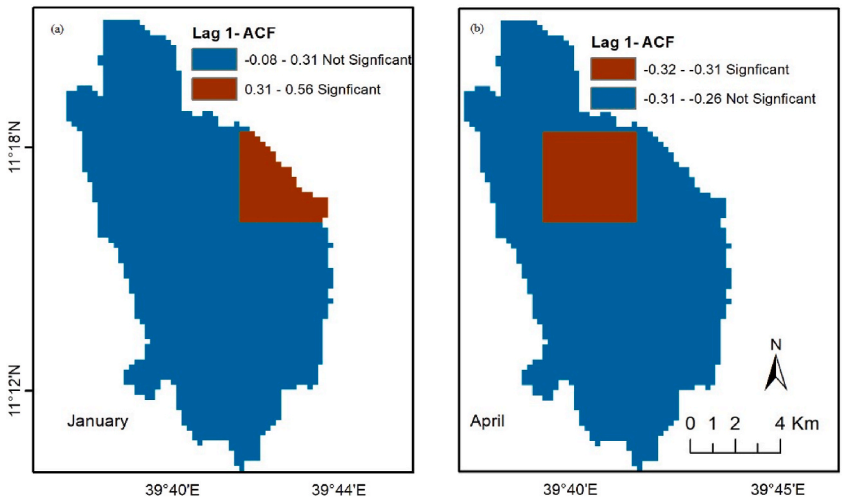

Fig. 9. Spatial (pixel-by-pixel) lag-1 serial correlation test result for monthly TAMSAT rainfall for January (a) and April (b) in Upper Gelana Watershed (1983–2021).

Table 5
Mann Kendall and Sen's slope (mm/year) test statistics for monthly rainfall (1983–2021) in the upper Gelana watershed calculated using TAMSAT data.

Month	LWD			UWD			*Dega*		
	Z-Value	Sen's slope	P-value	Z-Value	Sen's slope	P-value	Z-Value	Sen's slope	P-value
Jan	−0.18	0.00	0.856	−0.60	0.00	0.548	−0.57	0.00	0.567
Feb	−1.23	0.00	0.219	−0.82	0.00	0.412	−0.67	0.00	0.504
Mar	−1.43	−1.11	0.153	−1.39	−1.03	0.164	−1.19	−0.86	0.236
Apr	−0.64	−0.50	0.521	−0.48	−0.37	0.628	−0.48	−0.50	0.628
May	0.22	0.08	0.828	0.07	0.05	0.942	0.00	0.00	1.000
Jun	1.78	0.51	0.075*	2.12	0.65	0.034**	1.88	0.67	0.061*
Jul	2.23	3.29	0.026**	2.42	3.71	0.016**	2.18	3.65	0.029**
Aug	2.85	3.79	0.004**	2.82	3.79	0.005**	2.88	3.91	0.004**
Sep	2.17	1.26	0.030**	2.27	1.50	0.023**	1.69	1.39	0.090*
Oct	2.14	0.99	0.033**	1.80	0.77	0.071*	2.45	0.72	0.014**
Nov	2.00	0.01	0.045**	2.13	0.01	0.033**	1.96	0.21	0.050**
Dec	−1.24	0.00	0.213	−1.36	0.00	0.175	−1.51	0.00	0.132

* and ** indicate statistically significant at 0.1 and 0.05 alpha levels respectively.

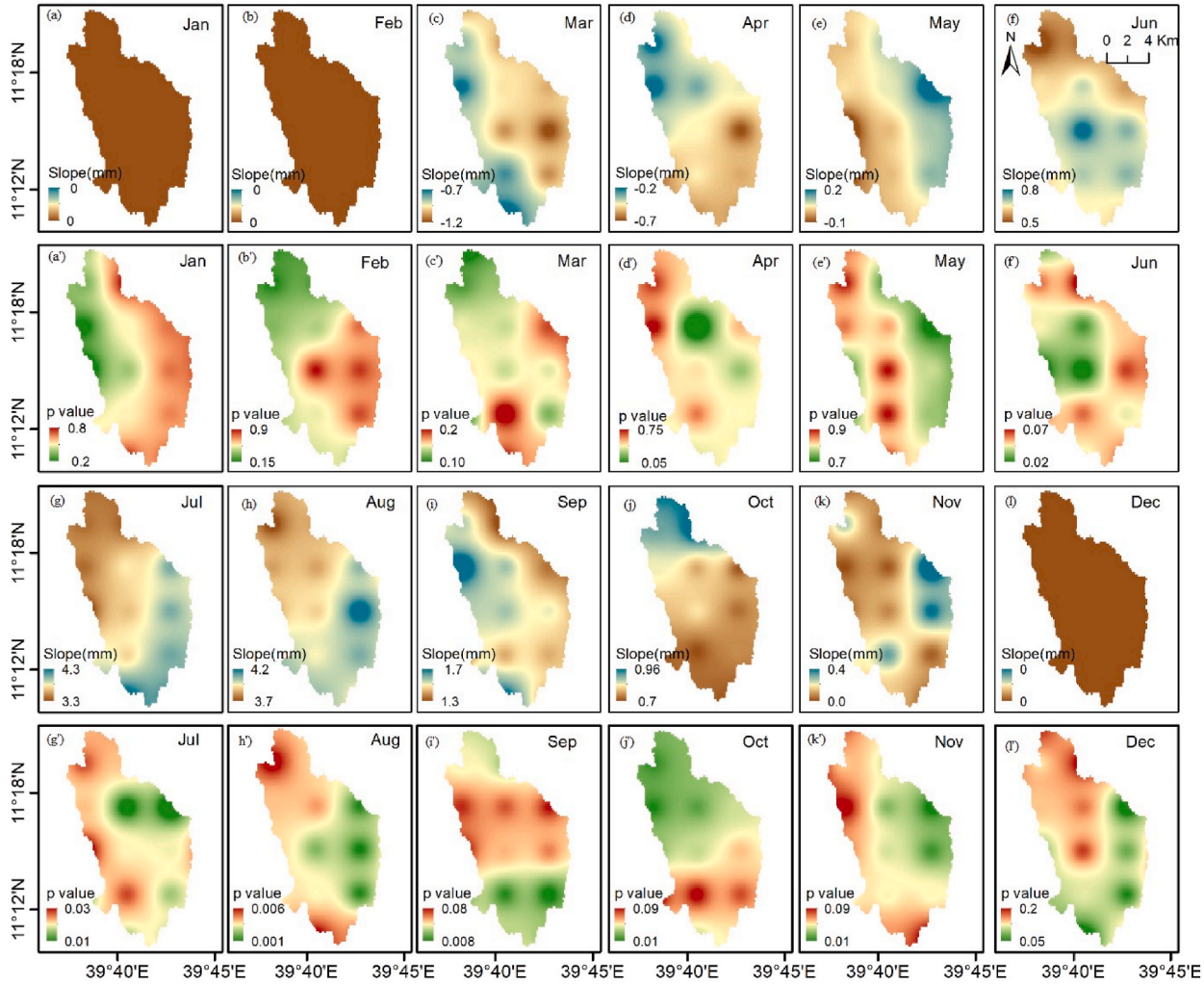

Fig. 10. Spatial patterns of Sen's slope expressed in mm/year (a–l) and significance of MK trends (a'-l') of monthly rainfall (1983–2021) in the upper Gelana watershed computed based on TAMSAT data.

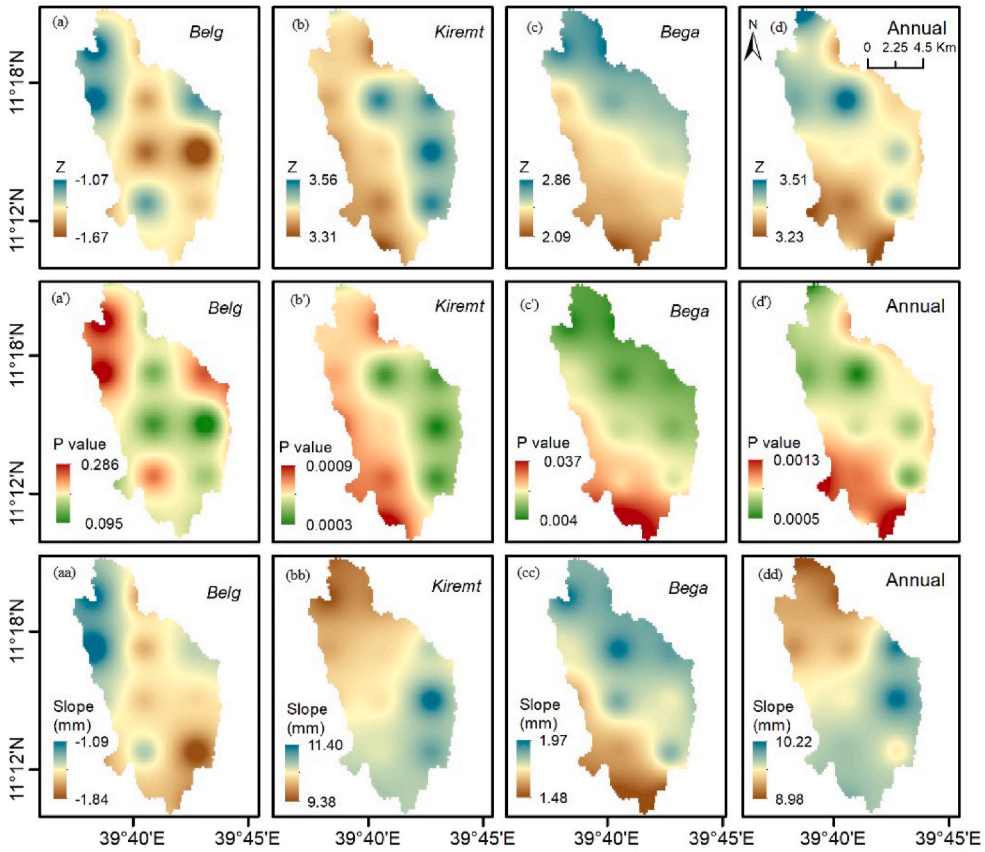

Fig. 11. Pixel-wise Mann Kendall trend (Z) (a–d), significance level (a'- d'), and Sen's slope in mm/year (aa-dd) for *belg*, *kiremt*, *bega* and annual rainfall (1983–2021) in the upper Gelana watershed calculated using TAMSAT data.

sequence, in LWD, UWD, and *dega* agroecology zones, during the study period (1983–2018).

3.5. Spatiotemporal trends of temperature

3.5.1. Monthly temperature trend analysis using MK

Before running Mann-Kendall and Sen's slope test, lag-1 serial correlation was computed for the monthly, seasonal, and annual average minimum, maximum, and mean temperature. Then, the pre-whitening procedure was applied for those time scales with a significant lag-1 serial correlation.

The MK test result shows a decreasing trend of monthly minimum temperatures for all months except November in the LWD and UWD agroecology zones (Table 8). In *dega* agroecology, a decreasing trend of the minimum temperature was detected in January, February, March, July, and November. On the contrary, the monthly maximum temperature shows a significant increasing trend in all months except November in the LWD and UWD agroecology zones. As shown in Table 8, the monthly maximum temperature in *dega* agroecology showed a positive trend from January to April and August months, while the other months exhibit a negative trend. Warming trends in the maximum temperature were reported by other authors [25,76,80]. A rising trend was observed in the monthly mean temperature in most of the months, with the exception of February and November in LWD and UWD and January, February, July, and November in the *dega* agroecology zones. Similar trends in minimum temperature were found in recent studies for different parts of Ethiopia [25,59,81]. [81] noted a declining trend for the monthly minimum temperature for Dessie.

3.5.2. Seasonal and annual temperature trends using MK

The seasonal and annual minimum temperature in LWD and UWD agroecology zones showed a statistically significant declining trend except in the *bega* season (Fig. 15a-l). In *dega* agroecology, declining trends were observed in the *belg* and annual timescales. Based on the Sen Slope statistics presented in Fig. 15j–k, the annual minimum temperature declines at a rate of approximately 0.3 °C per decade in both LWD and UWD agroecological zones. Similarly, declining trends in the seasonal and annual minimum temperatures were reported for the western parts of the upper Blue Nile river basin [25]. As shown in Fig. 16a-l, the seasonal and annual trends in maximum temperature varies across the study agroecological zones. In the LWD and UWD agroecological zones, the annual maximum temperature showed a significant rising trend at a decadal rate of 0.4 °C (Fig. 16j–k). The increments in the *belg* and annual maximum

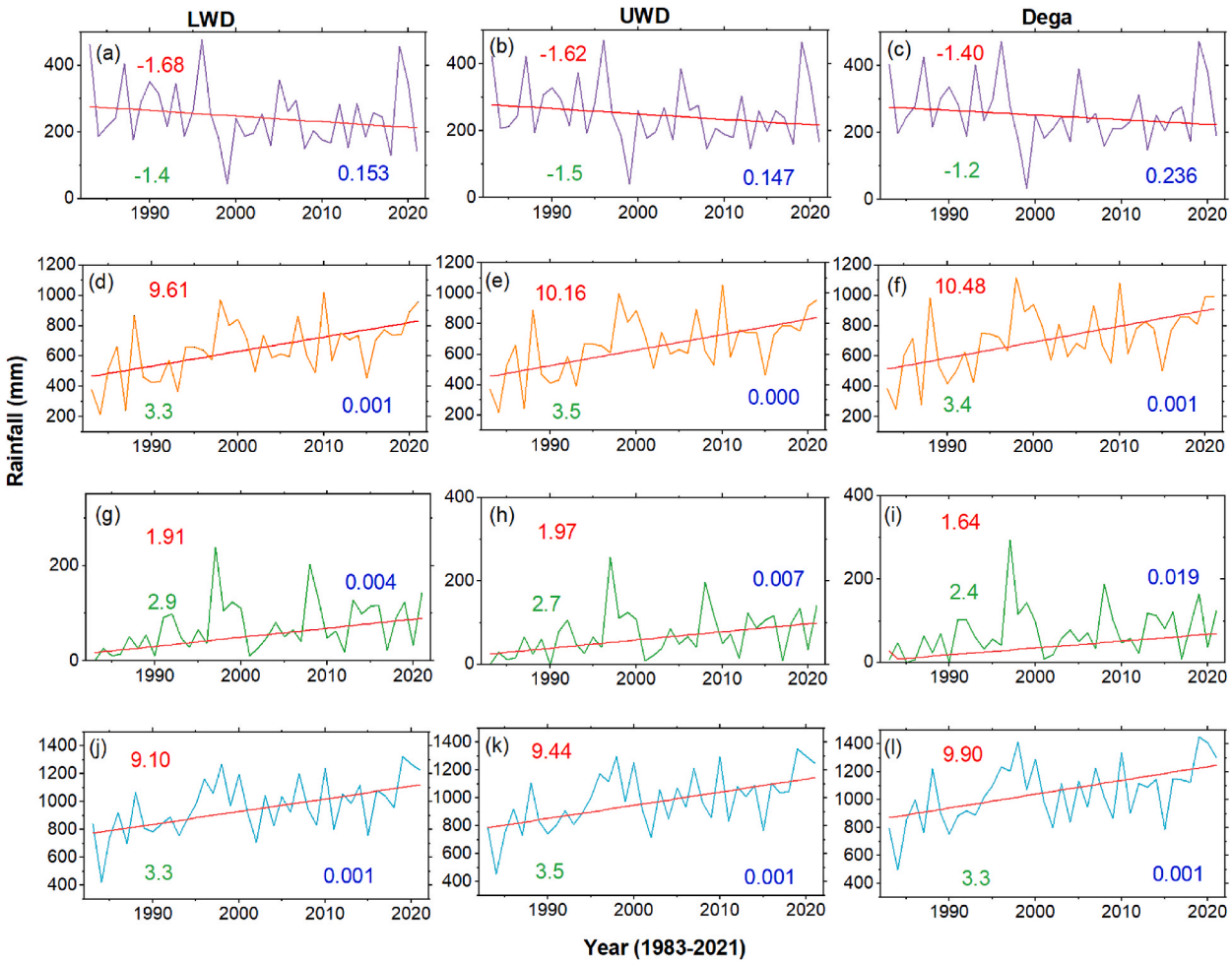

Fig. 12. Shows *belg* (a–c), *kiremt* (d–f), *bega* (g–i), and annual (j–l) rainfall trends (1983–2021) in the LWD (left), UWD (middle), and *dega* (right columns) agroecology zones of the upper Gelana watershed computed based on TAMSAT data. The zigzag lines represent rainfall (mm), and the straight line in red represents Sen's estimate of rainfall. In addition, the texts in green, red, and blue are the Z-value, Sen's slope (mm/year), and p-value of the MK test, respectively. (For interpretation of the references to color in this figure legend, the reader is referred to the Web version of this article.)

temperature in the *dega* agroecology were insignificant. As shown in Fig. 17a-l, insignificant positive trends were also observed in the seasonal and annual mean temperature except in the *bega* season in all the agroecology zones.

3.5.3. ITA for seasonal and annual temperature

As shown in Fig. 18a-l and Table 9, the seasonal and annual minimum temperatures are consistently declining across all clusters in the LWD and UWD. The seasonal and annual minimum temperatures in the *dega* agroecology zone exhibit an increasing tendency in the low clusters, but a declining trends were identified in the high clusters except for the *belg* season. The seasonal and annual maximum temperatures in LWD and UWD showed an increasing trend in all the clusters (Fig. 19a-l and Table 9). In the *dega* agroecology, *belg* and annual maximum temperatures showed a decreasing and increasing trend, respectively, in the high cluster (Table 9). In the low cluster, the annual mean temperature showed an increasing trend in all the agroecology zones (Fig. 20a-l and Table 9). Similarly, the *belg* and *kiremt* mean temperature showed an increasing trend in the *dega* agroecology. In the medium cluster, no trend was identified in the seasonal and annual mean temperature in all three agroecology zones. The seasonal and annual mean temperatures, with the exception of the *belg*, exhibited a declining tendency in the high cluster in the LWD and UWD agroecology zones. Whereas in *dega* agroecology, no trends were detected for seasonal and annual mean temperature in the high cluster data points (Fig. 20 and Table 9).

3.5.4. Comparison of MK and ITA for seasonal and annual temperature trends

The MK and ITA results completely match in the direction of trends for seasonal and annual minimum (decreasing) and maximum (increasing) temperatures in LWD and UWD agroecology zones. However, there is no clear match between the findings from the ITA

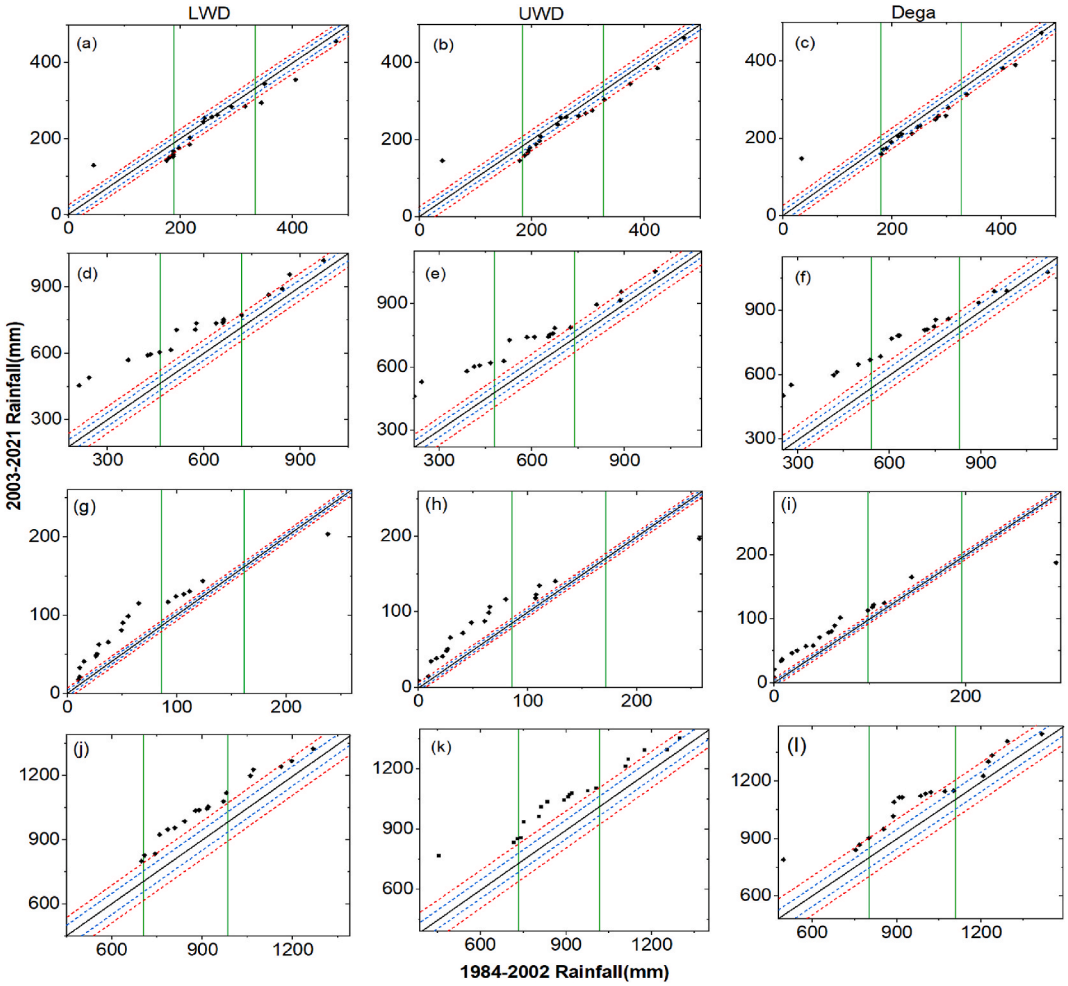

Fig. 13. Innovative trend analysis (ITA) results of the *belg* (a–c), *kiremt* (d–f), *bega* (g–i), and annual (j–l) rainfall (1984–2021) in the LWD (left), UWD (middle), and *dega* (right columns) agroecology zones of the upper Gelana watershed based on the TAMSAT data. Points in black color represent data points, the dash lines in red are the ±10% error and dash lines blue are ±5% error line and the line in black in between is the no-trend line. The green lines divide the data points into low, medium and high clusters. (For interpretation of the references to color in this figure legend, the reader is referred to the Web version of this article.)

and MK for the seasonal and annual minimum and maximum temperatures in the *dega* agroecology. For the seasonal and annual mean temperature, the MK shows statistically insignificant positive trends in all the agroecology zones, except for the *bega* season. Whereas the ITA results show no trends in mean temperature for the *belg* season in all the agroecology zones, except for the positive trend in the low cluster in the *dega* agroecology. The *kiremt* and annual mean temperatures also show no trend in the medium and high clusters in all agroecology zones, except for the declining trend in the high clusters in the LWD and UWD agroecology zones. Some contradicting findings of MK and ITA methods were also reported in an earlier study [35]. The comparison of the results shows that most of the insignificant negative and positive trends in the MK trend test tend to be trendless in the ITA method.

Points in black color represent data points, the dash lines in red are the ±10% error and dash lines blue are ±5% error line and the line in black in between is the no-trend line. The green lines divide the data points into low, medium and high clusters.

3.6. Farmer's perception on climate variability and trends

The results of the focus group discussion and interview confirmed the decreasing trend in *belg* rainfall. The participants reported that the decreasing (or total absence, as they described) of rainfall in the *belg* season hampered their efforts to become self-sufficient in food and caused a shortage of fodder for animals. A farmer in Amumo, a village in the upper *weina dega* (UWD) agroecology zone, told us, "In the past year, particularly before 1990, the yield we got from the *belg* season constituted a major part of food grain for household consumption, but nowadays we are not growing crops due to the lack of rainfall". Another informant also strengthens this idea by saying, "In the *belg* season it was possible to grow all the grains such as wheat (*Triticum aestivum*), barley (*Hordeum vulgare* L.), *teff* (*Eragrostis tef*) and others that we produce during the *kiremt* season, and sometimes we even harvest more than the *kiremt* season.

Table 6
Innovative trend analysis (ITA) statistics and cluster based interpretation of Fig. 13(a–l) for seasonal and annual rainfall (1984–2021) in the LWD, UWD and *dega* agroecological zones of the upper Gelana watershed using the TAMSAT data.

Agroecology	Timescale	Interpretation		
		Low	Medium	High
LWD	*Belg*	-*	-*	-*
	Kiremt	+*	+*	+*
	Bega	+*	+*	-*
	Annual	+*	+*	+*
UWD	*Belg*	-*	-*	-
	Kiremt	+*	+*	+*
	Bega	+*	+*	-*
	Annual	+*	+*	+*
Dega	*Belg*	+*	-	0
	Kiremt	+*	+*	-*
	Bega	+*	+*	-*
	Annual	+*	+*	+

Note: (−), (+) and (0) signs indicates decreasing, increasing and no trend, respectively and * indicate significant trend (points are outside of the ±5 error line).

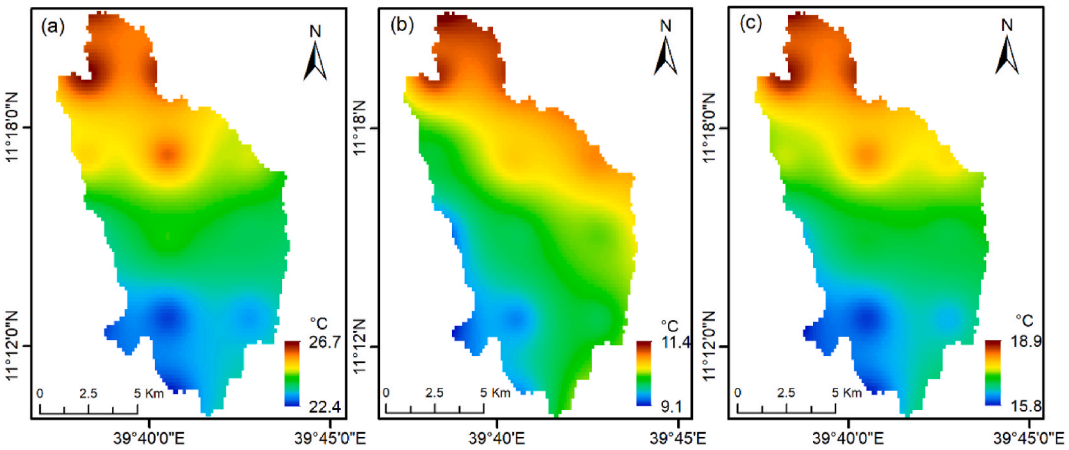

Fig. 14. Average maximum (a), minimum (b), and mean temperatures (°C) in the Upper Gelana watershed based on the gridded temperature from EMI (1983–2018).

However, the *belg* season is becoming completely dry, and we are no longer engaged in crop farming at this time".

Concerning the *kiremt* season, the informants' perspectives contradict the results of the statistical analysis of meteorological data. We found inconsistencies among the participants regarding the onset and termination of the *kiremt* season during the focus group discussion. The majority of them agree on the late start of rainfall, but they have different views on the cessation of *kiremt* rainfall. Some say it ends up early, while others say it terminates late. Nevertheless, both scenarios may have an impact on the farmer's agricultural practices. "In the past year, we sowed wheat starting from the second week of July, but in recent years it has shifted to the last week of July and sometimes the first week of August," an elderly person from Lay-Golbo (*dega* agroecology) village told us. The Mann-Kendall test results, on the other hand, show an increasing trend in rainfall across all four months of the *kiremt* season. But this is apparently related to the ITA findings, which reveal a decreasing trend in *kiremt* season rainfall, especially in the high cluster for the *dega* agroecology zone. Nonetheless, the perception of farmers about climate change is dependent on personal and environmental factors, so discrepancies may occur with findings that are based on meteorological data analysis [82]. Most of the time, their opinions are based on the most recent event they recall or that has an impact on their farming activities, rather than the cumulative effect of a long-term event.

The focus group discussants also pointed out that the temperature in their area is becoming hot. The informants also have similar perceptions regarding the increase in temperature. An informant from the Amumo village in the UWD reported that "there is no doubt that the temperature in our area has been increasing and no evidence for this other than looking at our environment. Plants such as kinchib (*Euphorbia tirucalli* L.) and banana were growing in hot temperatures, but nowadays they can grow in our village". During the field visit, we also noticed kinchib trees used as a fence and banana trees in some homesteads.

Table 7
Descriptive statistics of seasonal and annual average maximum, minimum and mean temperature (°C) from 1983 to 2018 for the Upper Gelana watershed based on the gridded temperature from EMI.

Time-scale	LWD						UWD						*Dega*					
	Min		Max		Avg		Min		Max		Avg		Min		Max		Avg	
	Mean	SD	Mean	SD	Mean	SD	Mean	SD	Mean	SD	Mean	SD	Mean	SD	Mean	SD	Mean	SD
Belg	11.5	1.1	26.9	1.1	19.2	0.5	10.9	1.1	26.3	1.1	18.6	0.5	9.8	0.9	22.8	0.7	16.3	0.4
Kiremt	13.5	0.6	27.9	0.5	20.7	0.3	12.9	0.6	27.3	0.5	20.1	0.3	11.4	0.5	23.9	0.5	17.6	0.3
Bega	8.1	1.4	24.8	1.2	16.5	0.9	7.6	1.4	24.2	1.2	15.9	0.9	6.8	1.2	20.8	1.0	13.8	0.8
Annual	11.0	0.7	26.6	0.6	18.8	0.4	10.5	0.7	26.0	0.6	18.2	0.4	9.3	0.6	22.6	0.4	15.9	0.3

Table 8
Summary of Mann-Kendall and Sen's slope test statistics for the maximum, minimum and mean temperature (°C) at monthly time scales for the LWD, UWD and *dega* agroecological zones (1983–2018) based on the gridded temperature from EMI.

Month	LWD			UWD			*Dega*		
	Min	**Max**	**Mean**	**Min**	**Max**	**Mean**	**Min**	**Max**	**Mean**
Jan	−0.031	0.038**	0.006	−0.032	0.038**	0.006	−0.046	0.025	−0.008
Feb	−0.092**	0.080***	−0.004	−0.093**	0.083***	−0.004	−0.032	0.032	−0.003
Mar	−0.085**	0.086***	−0.008	−0.084***	0.086***	−0.006	−0.002	0.031	0.010
Apr	−0.030	0.071***	0.016	−0.029	0.072***	0.016	0.018	0.005	0.008
May	−0.017	0.044**	0.012	−0.017	0.045**	0.013	0.018**	−0.000	0.009**
Jun	−0.026*	0.030***	0.001	−0.026**	0.033***	0.002	0.007	−0.011	0.001
Jul	−0.024**	0.027*	0.003	−0.024**	0.026*	0.004	−0.004	−0.014	−0.006
Aug	−0.015*	0.017*	0.001	−0.015*	0.019*	0.003	0.001	0.010	0.008
Sep	−0.025**	0.035***	0.007	−0.024*	0.038***	0.007	0.017	−0.006	0.011**
Oct	−0.013	0.039***	0.009	−0.015	0.039***	0.010	0.047**	−0.024*	0.013
Nov	0.039	0.010	0.025**	0.037	0.012	0.025*	−0.007	−0.012	−0.009

(−) indicates decreasing trend, *, ** and *** indicate statistically significant at 0.1, 0.05 and 0.01 alpha levels, respectively.

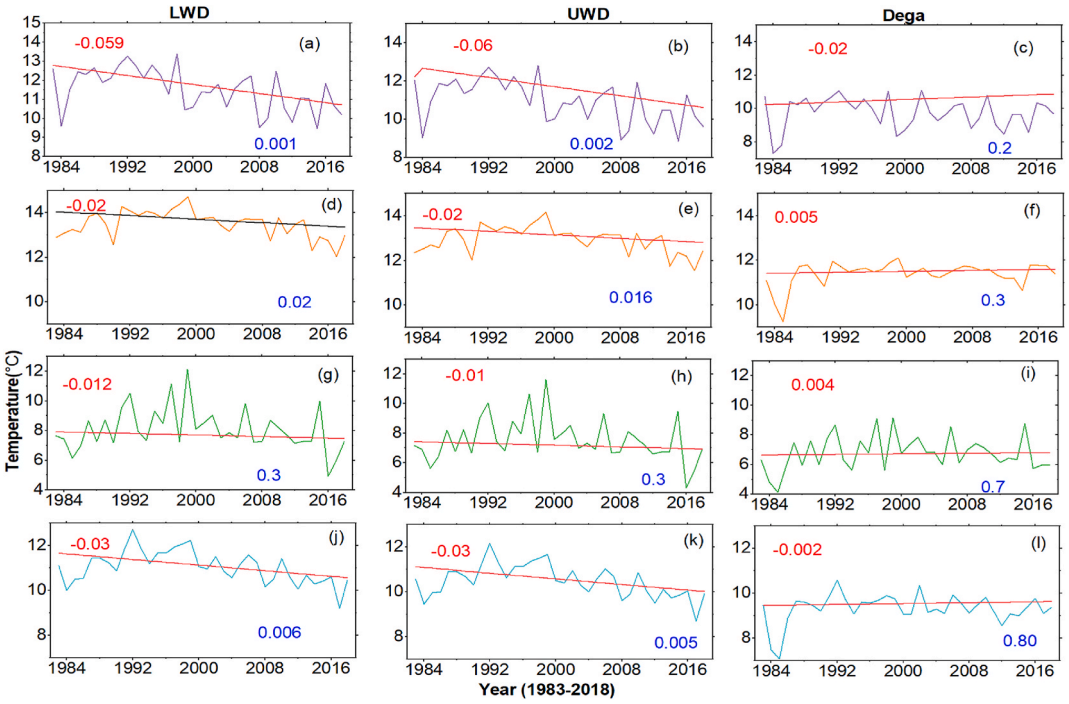

Fig. 15. Shows *belg* (a–c), *kiremt* (d–f), *bega* (g–i), and annual (j–l) minimum temperature trends (1983–2018) in the LWD (left), UWD (middle), and *dega* (right columns) agroecology zones of the upper Gelan watershed based on the gridded temperature from EMI. The zigzag lines represent actual temperature, and the straight line in red represents Sen's estimate. In addition, the texts red and blue are the Sen's slope (°C/year) and p-value of the MK test, respectively. (For interpretation of the references to color in this figure legend, the reader is referred to the Web version of this article.)

4. Conclusions

In this study, we found that TAMSAT has a relatively low average magnitude of errors compared to CHIRPS, and a better correlation with the daily rainfall from ground-based stations. The POD revealed that TAMSAT has a better ability to detect daily rainfall. The ETS demonstrates that the daily rainfall estimate from TAMSAT has better correspondence with gauged rainfall. In addition, FAR was lower in TAMSAT's daily rainfall, and the frequency of daily rain events in TAMSAT was very close to the frequencies of daily gauged rainfall. Moreover, HSS suggests that TAMSAT has better skill or accuracy than CHIRPS in daily rainfall estimates. Regarding the monthly rainfall, the categorical evaluation statistics revealed the two products have comparable performances, with CHIRPS slightly performing better than TAMSAT.

The study area is characterized by a strongly irregular distribution of rainfall throughout the study period. Based on TAMSAT rainfall product, we found a significant increasing trend in monthly rainfall from June to November in the LWD, UWD and *dega* agroecology zones using the MK test. However, a slightly different trend was detected in the pixel-wise trend analysis in the March and

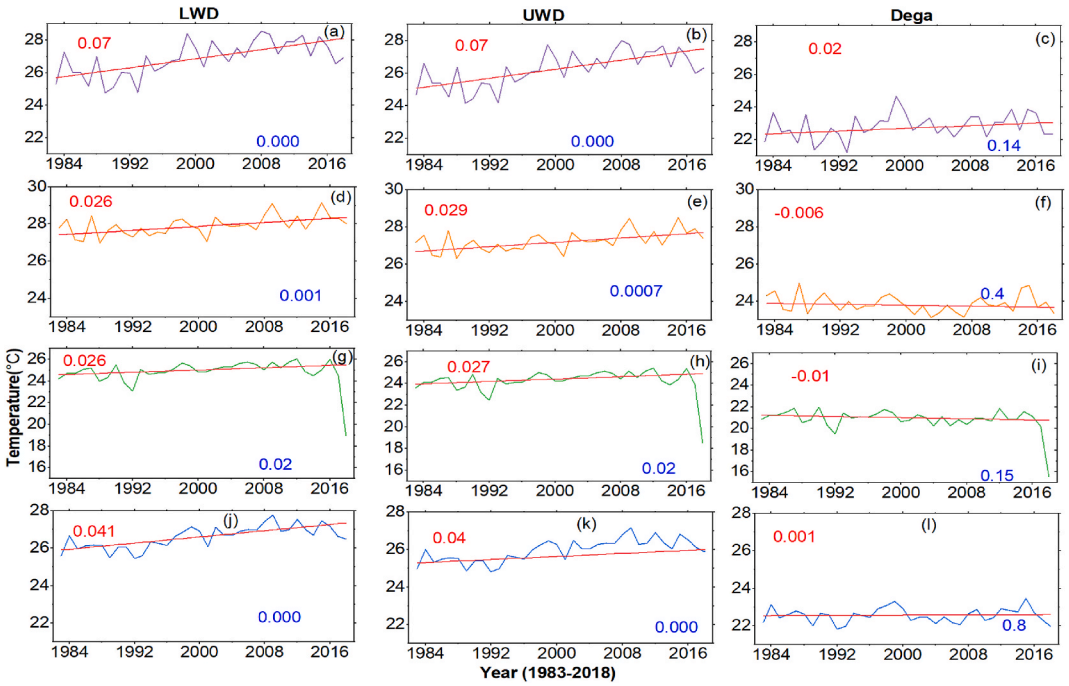

Fig. 16. Shows *belg* (a–c), *kiremt* (d–f), *bega* (g–i), and annual (j–l) maximum temperature trends (1983–2018) in the LWD (left), UWD (middle), and *dega* (right columns) agroecology zones of the upper Gelana watershed based on gridded temperature data from EMI. The zigzag lines represent actual temperature, and the straight line in red represents Sen's estimate. In addition, the texts red and blue are the Sen's slope (°C/year) and p-value of the MK test, respectively. (For interpretation of the references to color in this figure legend, the reader is referred to the Web version of this article.)

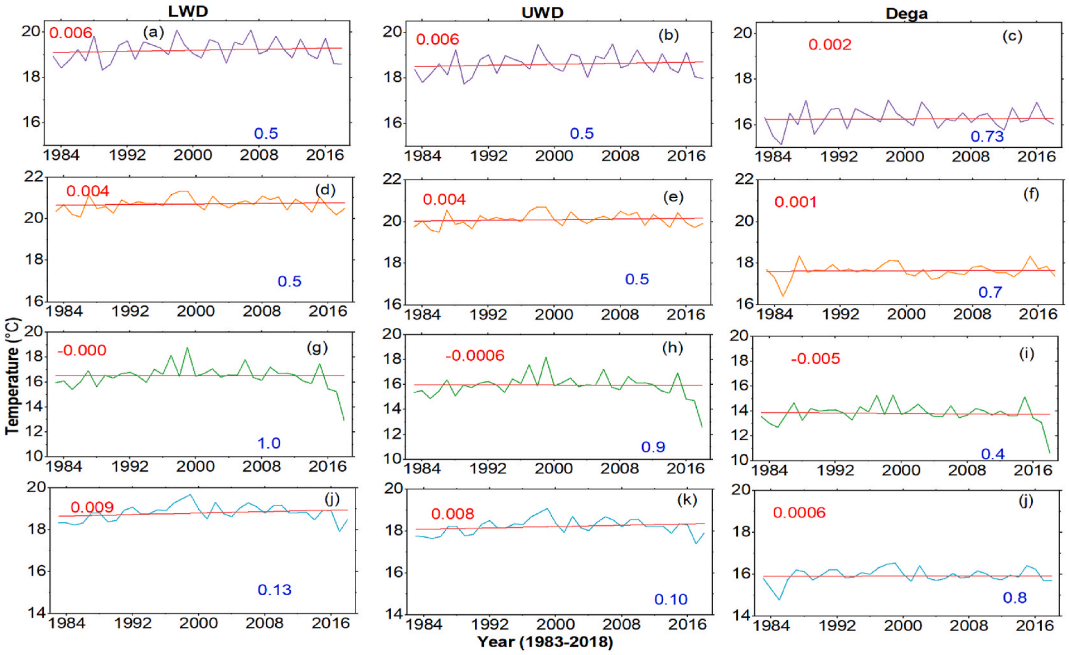

Fig. 17. Shows *belg* (a–c), *kiremt* (d–f), *bega* (g–i), and annual (j–l) mean temperature trends (1983–2018) in the LWD (left), UWD (middle), and *dega* (right columns) agroecology zones of the upper Gelana watershed based on the gridded temperature data from EMI. The zigzag lines represent actual temperature, and the straight line in red represents Sen's estimate. In addition, the texts red and blue are the Sen's slope (°C/year) and p-value of the MK test, respectively. (For interpretation of the references to color in this figure legend, the reader is referred to the Web version of this article.)

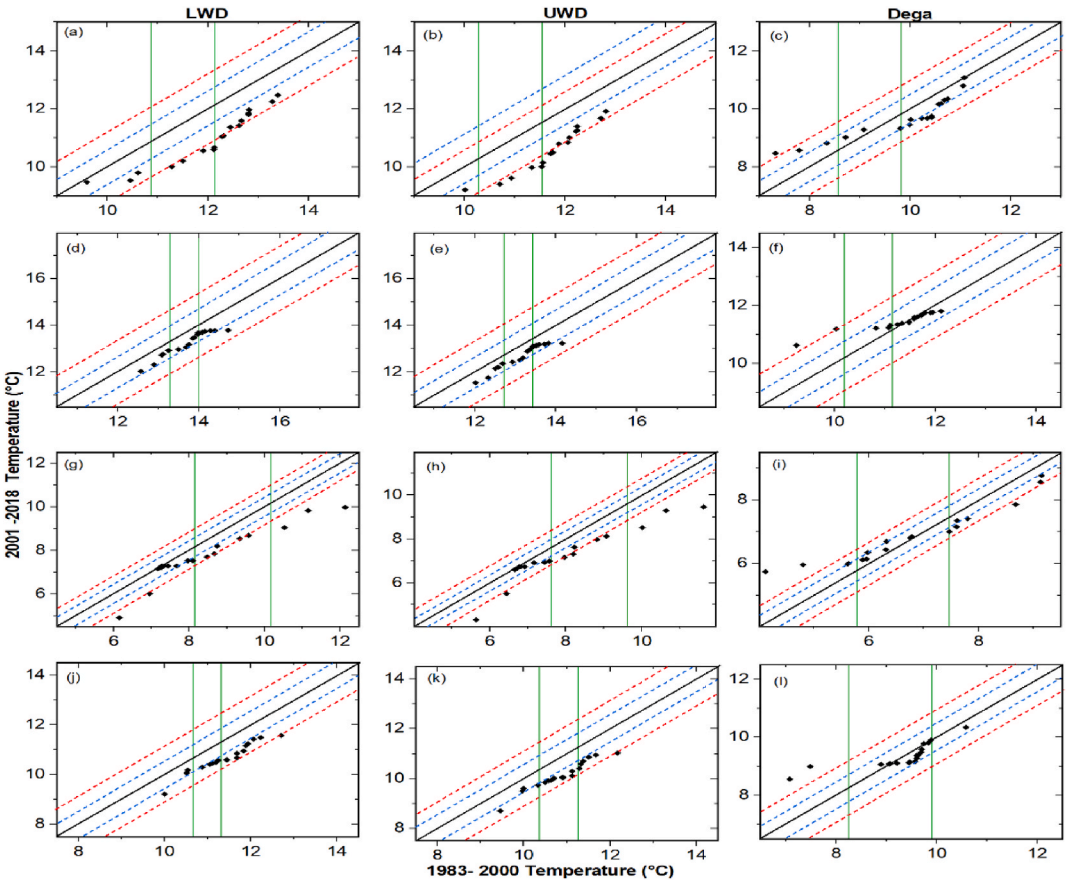

Fig. 18. Shows the innovative trend analysis (ITA) of the *belg* (a–c), *kiremt* (d–f), *bega* (g–i), and annual (j–l) minimum temperature (1983–2018) in the LWD (left), UWD (middle), and *dega* (right columns) agroecology zones of the upper Gelana watershed based on the gridded temperature data from EMI.

Table 9
Summary interpretation of the innovative trend analysis (ITA) of minimum, maximum and mean temperatures (°C) for the Upper Gelana watershed (Figs. 18–20).

		LWD				UWD				*Dega*			
	Clusters	*Belg*	*Kiremt*	*Bega*	Annual	*Belg*	*Kiremt*	*Bega*	Annual	*Belg*	*Kiremt*	*Bega*	Annual
Minimum	Low	-*	–	-*	–	-*	–	-*	-*	+	+*	+	+*
	Medium	-*	–	-*	-*	-*	–	-*	-*	–	+	0	0
	High	-*	-*	-*	-*	-*	-*	-*	-*	0	–	-*	–
Maximum	Low	+*	+	+	+	+*	+	+	+	+	–	0	0
	Medium	+	+	+	+	+	+	+	+	0	–	–	0
	High	+	+	+	+	+	+	+	+	–	0	0	+
Mean	Low	0	0	0	+	0	0	0	+	+	+	0	+
	Medium	0	0	0	0	0	0	0	0	0	0	0	0
	High	0	–	-*	–	0	–	-*	–	0	0	0	0

(−), (+) and (0) signs indicates decreasing, increasing and no trend, respectively and * indicate significant trends (points are outside of the ±5 error line).

May months for some parts of the stud area. We found a significant positive trend in the *kiremt* season and annual rainfall that vary across the study area. In contrast, rainfall during the *belg* season shows a statistically insignificant downward trend and high variability. The increment in *kiremt* season and annual rainfall is higher in the *dega* agroecology zone and lower in the LWD. The findings from MK and ITA agree in showing the directions of trends in *belg* and *kiremt* season rainfall in the LWD and UWD and annual trends in all the agroecology zones. A few contrasting findings were found using the ITA method, which can be considered as having the ability to detect trends that are hidden in the MK test.

In all the agroecological zones of the study area, mean monthly temperatures were low in December and high in June during the

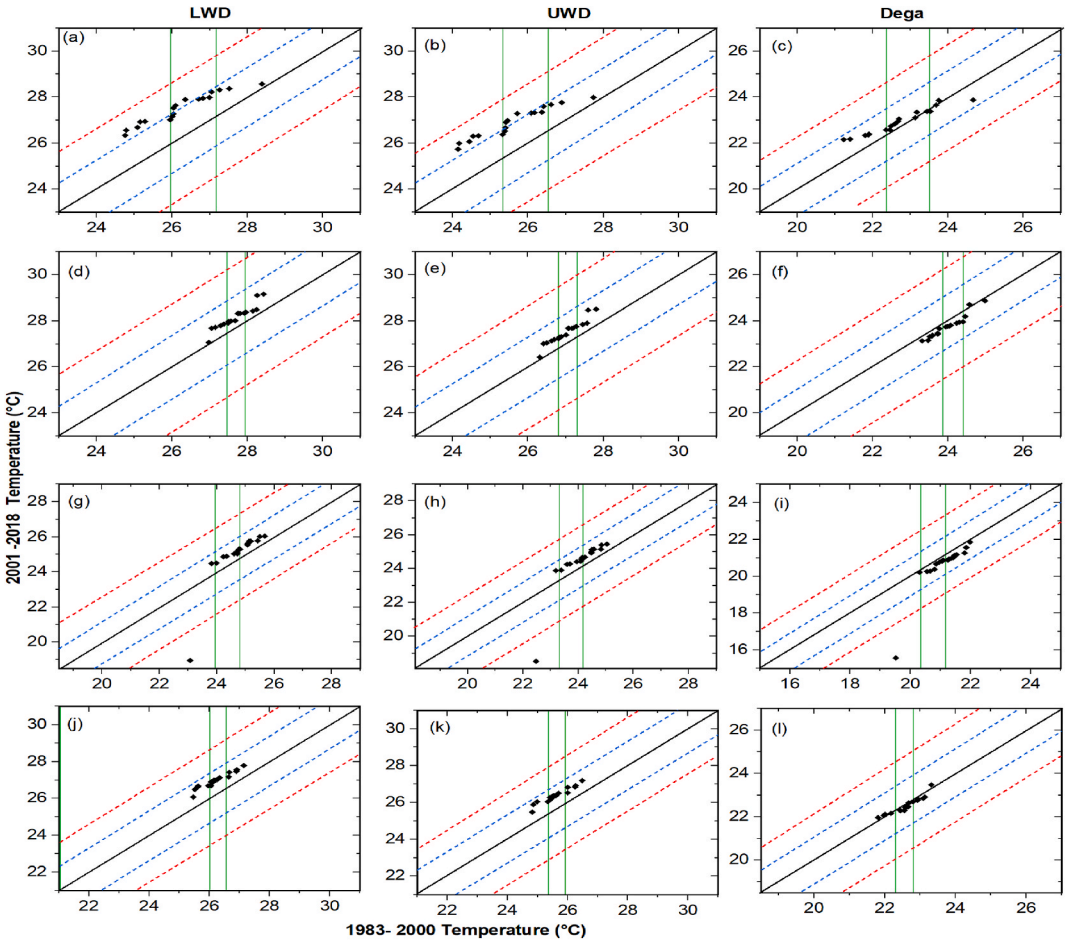

Fig. 19. Shows the innovative trend analysis (ITA) of the *belg* (a–c), *kiremt* (d–f), *bega* (g–i), and annual (j–l) maximum temperature (1983–2018) in the LWD (left), UWD (middle), and *dega* (right columns) agroecology zones of the upper Gelana watershed based on the gridded temperature data from EMI. Points in black color represent data points, the dash lines in red are the ±10% error and dash lines blue are ±5% error line and the line in black in between is the no-trend line. The green lines divide the data points into low, medium and high clusters. (For interpretation of the references to color in this figure legend, the reader is referred to the Web version of this article.)

study period (1983–2018). The seasonal average maximum, minimum, and mean temperatures were high in the *kiremt* season. The MK test shows that the monthly minimum and maximum temperatures, in order of sequence, showed significant declining and warming trends in most months in the LWD and UWD agroecology zones. The majority of months in *dega* agroecology exhibit an insignificant upward trend in both temperatures. With the exception of the *kiremt* and *bega* seasons in *dega* agroecology, the seasonal and annual minimum and maximum temperatures, respectively, showed decreasing and increasing trends in all the agroecology zones. However, these trends are significant only in LWD and UWD agroecology zones. The MK-based trends in seasonal and annual minimum and maximum temperatures are in agreement with the ITA-based trends in the LWD and UWD, but some discrepancies were found in the case of the *dega* agroecology zone. The findings suggest the need to implement adaptation programs to make sure communities are safe from the possible impacts of climate change and variability.

Funding statement

This research was funded by the Office of the Vice President for Research and Technology Transfer (VPRTT), Addis Ababa University, Addis Ababa, Ethiopia and Regional Center for Mapping of Resources for Development (RCMRD)/GMES and Africa, Nairobi, Kenya.

Data availability statement

The data, excluding the meteorological data from EMI, will be made available by the corresponding author upon request.

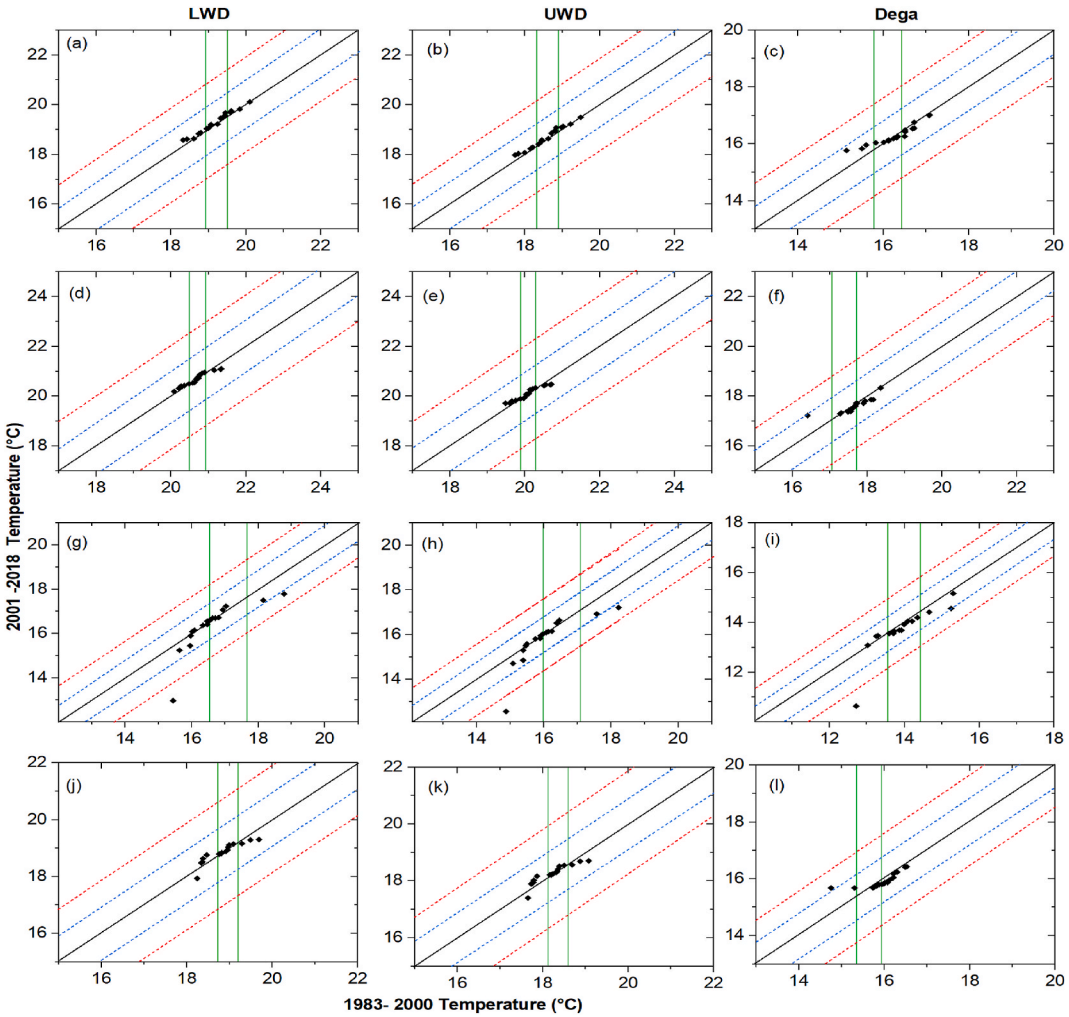

Fig. 20. Shows the innovative trend analysis (ITA) of the *belg* (a–c), *kiremt* (d–f), *bega* (g–i), and annual (j–l) mean temperature (1983–2018) in the LWD (left), UWD (middle), and *dega* (right columns) agroecology zones of the upper Gelana Watershed computed using the gridded temperature data from EMI. Points in black color represent data points, the dash lines in red are the ±10% error and dash lines blue are ±5% error line and the line in black in between is the no-trend line. The green lines divide the data points into low, medium and high clusters. (For interpretation of the references to color in this figure legend, the reader is referred to the Web version of this article.)

CRediT authorship contribution statement

Sileshi Tadesse: Conceptualization, Data curation, Formal analysis, Funding acquisition, Investigation, Methodology, Project administration, Resources, Software, Validation, Visualization, Writing – original draft, Writing – review & editing. **Asnake Mekuriaw:** Conceptualization, Formal analysis, Funding acquisition, Investigation, Methodology, Project administration, Resources, Software, Supervision, Validation, Writing – original draft, Writing – review & editing. **Mohammed Assen:** Conceptualization, Data curation, Funding acquisition, Investigation, Methodology, Project administration, Resources, Software, Validation, Writing – review & editing.

Declaration of competing interest

The authors declare that they have no known competing financial interests or personal relationships that could have appeared to influence the work reported in this paper.

Acknowledgments

The first author expresses gratitude to Addis Ababa University and the Regional Center for Mapping of Resources for Development (RCMRD)/GMES and Africa for their financial support during this study. The authors also extend their thanks to the Tehuledera

District Agricultural and Rural Development Office, development agents, and farmers who participated in the interviews and focus group discussions. Special appreciation is also extended to the Ethiopian Meteorological Institute (EMI) for providing precipitation and temperature data. Lastly, we would like to convey our heartfelt appreciation to the editor and reviewers whose contributions significantly enhanced this work.

References

[1] IPCC, Summary for policymakers, in: P.R.S. Masson-Delmotte, V, P. Zhai, H.-O. Pörtner, D. Roberts, J. Skea, M.I.G.A. Pirani, W. Moufouma-Okia, C. Péan, R. Pidcock, S. Connors, J.B.R. Matthews, Y. Chen, X. Zhou, T.W.E. Lonnoy, T. Maycock, M. Tignor (Eds.), Glob. Warm. 1.5°C. An IPCC Spec. Rep. Impacts Glob. Warm. 1.5°C above Pre-industrial Levels Relat. Glob. Greenh. Gas Emiss. Pathways, Context Strength. Glob. Response to Threat Clim. Chang., Cambridge University Press, Cambridge, UK, 2018, pp. 3–24, https://doi.org/10.1017/9781009157940.001.

[2] A. Costello, M. Abbas, A. Allen, S. Ball, S. Bell, R. Bellamy, S. Friel, N. Groce, A. Johnson, M. Kett, M. Lee, C. Levy, M. Maslin, D. McCoy, B. McGuire, H. Montgomery, D. Napier, C. Pagel, J. Patel, J.A.P. de Oliveira, N. Redclift, H. Rees, D. Rogger, J. Scott, J. Stephenson, J. Twigg, J. Wolff, C. Patterson, Managing the health effects of climate change. Lancet and University college London Institute for global health commission, Lancet 373 (2009) 1693–1733, https://doi.org/10.1016/S0140-6736(09)60935-1.

[3] M.E.S. Louis, J.J. Hess, Climate change. Impacts on and implications for global health, Am. J. Prev. Med. 35 (2008) 527–538, https://doi.org/10.1016/j.amepre.2008.08.023.

[4] M.M.Q. Mirza, Climate change and extreme weather events: can developing countries adapt? Clim. Pol. 3 (2003) 233–248, https://doi.org/10.3763/cpol.2003.0330.

[5] M.M. Majedul Islam, in: S.A. Bandh (Ed.), Threats to Humanity from Climate Change, Clim. Chang., Springer, Cham, 2022, pp. 21–36, https://doi.org/10.1007/978-3-030-86290-9_2.

[6] R.K. Upadhyay, Markers for global climate change and its impact on social, biological and ecological systems: a review, Am. J. Clim. Change 9 (2020) 159–203, https://doi.org/10.4236/ajcc.2020.93012.

[7] S. Bandh, S. Shafi, M. Peerzada, T. Rehman, S. Bashir, S.A. Wani, R. Dar, Multidimensional analysis of global climate change: a review, Environ. Sci. Pollut. Res. (2021), https://doi.org/10.1007/s11356-021-13139-7.

[8] T. Weber, P. Bowyer, D. Rechid, S. Pfeifer, F. Raffaele, A.R. Remedio, C. Teichmann, D. Jacob, Analysis of compound climate extremes and exposed population in Africa under two different emission scenarios, Earth's Future 8 (2020) 1–20, https://doi.org/10.1029/2019EF001473.

[9] A. Ayanlade, A. Oluwaranti, O.S. Ayanlade, M. Borderon, H. Sterly, P. Sakdapolrak, M.O. Jegede, L.F. Weldemariam, A.F.O. Ayinde, Extreme climate events in sub-Saharan Africa: a call for improving agricultural technology transfer to enhance adaptive capacity, Clim. Serv. 27 (2022), https://doi.org/10.1016/j.cliser.2022.100311.

[10] S. Chapman, C. E Birch, E. Pope, S. Sallu, C. Bradshaw, J. Davie, J. H Marsham, Impact of climate change on crop suitability in sub-Saharan Africa in parameterized and convection-permitting regional climate models, Environ. Res. Lett. 15 (2020), https://doi.org/10.1088/1748-9326/ab9daf.

[11] K. Joosten, S. Grey, Integrating Climate Change Adaptation and Mitigation into the Watershed Management Approach in Eastern Africa – Discussion Paper and Good Practices, FAO, Addis Ababa, 2017.

[12] C. Funk, A. Hoell, S. Nicholson, D. Korecha, G. Galu, G. Artan, F. Teshome, K. Hailermariam, Z. Segele, L. Harrison, A. Tadege, Z. Atheru, C. Pomposi, D. Pedreros, Examining the potential contributions of extreme "western v" sea surface temperatures to the 2017 March-June east african drought, Bull. Am. Meteorol. Soc. 100 (2018) S55–S60, https://doi.org/10.1175/BAMS-D-18-0108.1.

[13] S.F. Kew, S.Y. Philip, M. Hauser, M. Hobbins, N. Wanders, G. Jan Van Oldenborgh, K. Van Der Wiel, T.I.E. Veldkamp, J. Kimutai, C. Funk, F.E.L. Otto, Impact of precipitation and increasing temperatures on drought trends in eastern Africa, Earth Syst. Dyn. 12 (2021) 17–35, https://doi.org/10.5194/esd-12-17-2021.

[14] I. Hamza, A. Iyela, Land use pattern, climate change, and its implication for food security in Ethiopia: a review, Ethiop. J. Environ. Stud. Manag. 5 (2012) 26–31, https://doi.org/10.4314/ejesm.v5i1.4.

[15] D. Temesgen, H. Yehualashet, D.S. Rajan, Climate change adaptations of smallholder farmers in South Eastern Ethiopia, J. Agric. Ext. Rural Dev. 6 (2014) 354–366, https://doi.org/10.5897/JAERD14.0577.

[16] D. Conway, E.L.F. Schipper, Adaptation to climate change in Africa: challenges and opportunities identified from Ethiopia, Global Environ. Change 21 (2011) 227–237, https://doi.org/10.1016/j.gloenvcha.2010.07.013.

[17] World Bank, Ethiopia: Accelerating Equitable Growth, Country Economic Memorandum, World Bank, Washington, DC, 2007.

[18] G.A. Mera, Drought and its impacts in Ethiopia, Weather Clim. Extrem. 22 (2018) 24–35, https://doi.org/10.1016/j.wace.2018.10.002.

[19] A.Y. Kassaye, G. Shao, X. Wang, S. Wu, Quantification of drought severity change in Ethiopia during 1952–2017, Environ. Dev. Sustain. 23 (2021) 5096–5121, https://doi.org/10.1007/s10668-020-00805-y.

[20] A.A. Mekonen, A.B. Berlie, Spatiotemporal variability and trends of rainfall and temperature in the Northeastern Highlands of Ethiopia, Model. Earth Syst. Environ. (2019), https://doi.org/10.1007/s40808-019-00678-9.

[21] A. Asfaw, B. Simane, A. Hassen, A. Bantider, Variability and time series trend analysis of rainfall and temperature in northcentral Ethiopia : a case study in Woleka sub-basin, Weather Clim. Extrem. 19 (2018) 29–41, https://doi.org/10.1016/j.wace.2017.12.002.

[22] K. V Suryabhagavan, GIS-based climate variability and drought characterization in Ethiopia over three decades, Weather Clim. Extrem. 15 (2017) 11–23, https://doi.org/10.1016/j.wace.2016.11.005.

[23] M. Tadese, L. Kumar, R. Koech, Climate change projections in the awash river basin of Ethiopia using global and regional climate models, Int J Clim 40 (2020) 3649–3666, https://doi.org/10.1002/joc.6418.

[24] S. Gummadi, K.P.C. Rao, J. Seid, G. Legesse, M.D.M. Kadiyala, R. Takele, Spatio-temporal variability and trends of precipitation and extreme rainfall events in Ethiopia in 1980 – 2010, Theor. Appl. Climatol. (2017), https://doi.org/10.1007/s00704-017-2340-1.

[25] D. Mengistu, W. Bewket, R. Lal, Recent spatiotemporal temperature and rainfall variability and trends over the upper blue Nile river basin, Ethiopia, Int. J. Climatol. 34 (2014) 2278–2292, https://doi.org/10.1002/joc.3837.

[26] M. Gedefaw, D. Yan, T. Hao Wang, I. Qin, A. Girma, A. Abiyu, D. Batsuren, Innovative trend analysis of annual and seasonal rainfall variability in Amhara regional, Atmosphere 9 (2018) 1–10, https://doi.org/10.3390/atmos9090326.

[27] M.M. Alemu, G.T. Bawoke, Analysis of spatial variability and temporal trends of rainfall in Amhara region , Ethiopia melkamu meseret alemu and getnet taye bawoke, J. Water Clim. Chang. 11 (2020) 1505–1520, https://doi.org/10.2166/wcc.2019.084.

[28] A. Gebremichael, S. Quraishi, G. Mamo, Analysis of seasonal rainfall variability for agricultural water resource management in southern region , Ethiopia, J. Nat. Sci. Res. 4 (2014) 56–80.

[29] W. Bewket, D. Conway, A note on the temporal and spatial variability of rainfall in the drought-prone Amhara region of Ethiopia, Int. J. Climatol. 27 (2007) 1467–1477, https://doi.org/10.1002/joc.1481.

[30] G.T. Ayehu, T. Tadesse, B. Gessesse, T. Dinku, Validation of new satellite rainfall products over the upper blue nile basin, Ethiopia, Atmos. Meas. Tech. 11 (2018) 1921–1936, https://doi.org/10.5194/amt-11-1921-2018.

[31] T. Dinku, C. Funk, P. Peterson, R. Maidment, T. Tadesse, H. Gadain, P. Ceccato, Validation of the CHIRPS satellite rainfall estimates over eastern Africa, Q. J. R. Meteorol. Soc. 144 (2018) 292–312, https://doi.org/10.1002/qj.3244.

[32] X. Li, Q. Zhang, C.Y. Xu, Assessing the performance of satellite-based precipitation products and its dependence on topography over Poyang Lake basin, Theor. Appl. Climatol. 115 (2014) 713–729, https://doi.org/10.1007/s00704-013-0917-x.

[33] A. Saini, N. Sahu, Decoding trend of Indian summer monsoon rainfall using multimethod approach, Stoch. Environ. Res. Risk Assess. (2021), https://doi.org/10.1007/s00477-021-02030-z.

[34] R. Ali, A. Kuriqi, S. Abubaker, O. Kisi, Long-term trends and seasonality detection of the observed flow in yangtze river using mann-kendall and Sen's innovative trend method, Water 11 (2019) 1–17, https://doi.org/10.3390/w11091855.

[35] T. Caloiero, R. Coscarelli, E. Ferrari, Application of the innovative trend analysis method for the trend analysis of rainfall anomalies in southern Italy, water resour, Manag 32 (2018) 4971–4983, https://doi.org/10.1007/s11269-018-2117-z.

[36] L. Cui, L. Wang, Z. Lai, Q. Tian, W. Liu, J. Li, Innovative trend analysis of annual and seasonal air temperature and rainfall in the Yangtze River Basin, China during 1960 –2015, J. Atmos. Solar-Terrestrial Phys. 164 (2017) 48–59, https://doi.org/10.1016/j.jastp.2017.08.001.

[37] A. Girma, T. Qin, H. Wang, D. Yan, M. Gedefaw, A. Abiyu, D. Batsuren, Study on recent trends of climate variability using innovative trend analysis : the case of the upper huai river basin, Pol. J. Environ. Stud. 29 (2020) 2199–2210, https://doi.org/10.15244/pjoes/103448.

[38] H. Yang, H. Xiao, C. Guo, Y. Sun, R. Gao, Innovative trend analysis of annual and seasonal precipitation in Ningxia, China, Atmos, Ocean. Sci. Lett. 13 (2020) 1–8, https://doi.org/10.1080/16742834.2020.1752616.

[39] Z. Sen, Innovative trend analysis methodology, J. Hydrol. Eng. 7 (2012) 1042–1046, https://doi.org/10.1061/(ASCE)HE.1943-5584.0000556.

[40] H. Hurni, Agroecological Belts of Ethiopia: Explanatory Notes on Three Maps at Scale of 1:1, 000,000, 1998. Bern, Switzerland.

[41] M. Negash, The need for meteorological information to plan agroforestry on steep slopes in Ethiopia, in: W.E. Reifsnyder, T.O. Darnhofer (Eds.), Meteorol. Agrofor. Proc. An Int. Work. Appl. Meteorol. to Agrofor. Syst. Plan, . Manag., Nairobi, 1987, pp. 181–189.

[42] S. Rosell, M. Olvmo, B. Holmer, Cultivated land – a scarce commodity in a densely populated rural area in South Wollo, Ethiopia, J. Land Use Sci. 12 (2017) 252–270, https://doi.org/10.1080/1747423X.2017.1319978.

[43] T. Dinku, P. Ceccato, E. Grover-Kopec, M. Lemma, S.J. Connor, C.F. Ropelewski, Validation of satellite rainfall products over East Africa's complex topography, Int. J. Rem. Sens. 28 (2007) 1503–1526, https://doi.org/10.1080/01431160600954688.

[44] C. Funk, P. Peterson, M. Landsfeld, D. Pedreros, J. Verdin, S. Shukla, G. Husak, J. Rowland, L. Harrison, A. Hoell, J. Michaelsen, The climate hazards infrared precipitation with stations — a new environmental record for monitoring extremes, Sci. Data 2 (2015), https://doi.org/10.1038/sdata.2015.66.

[45] C. Aybar, Rgee: R Bindings for Calling the "Earth Engine" API. R Package, 2021, version 1.1.2. https://cran.r-project.org/package=rgee.

[46] R.I. Maidment, D. Grimes, R.P. Allan, E. Tarnavsky, M. Marcstringer, T. Hewison, R. Roebeling, E. Black, The 30 year TAMSAT african rainfall climatology and time series (TARCAT) data set, J. Geophys. Res. Atmos. Res. 119 (2014) 10619–10644, https://doi.org/10.1002/2014JD021927.

[47] E. Tarnavsky, D. Grimes, R. Maidment, E. Black, R.P. Allan, M. Stringer, R. Chadwick, F. Kayitakire, Extension of the TAMSAT satellite-based rainfall monitoring over Africa and from 1983 to present, J. Appl. Meteorol. Climatol. 53 (2014) 2805–2822, https://doi.org/10.1175/JAMC-D-14-0016.1.

[48] R.I. Maidment, D. Grimes, E. Black, E. Tarnavsky, M. Young, H. Greatrex, R.P. Allan, T. Stein, E. Nkonde, S. Senkunda, E.M.U. Alcántara, A new, long-term daily satellite-based rainfall dataset for operational monitoring in Africa, Sci. Data 4 (2017) 1–17, https://doi.org/10.1038/sdata.2017.63.

[49] B. Ebert, Forecast Verification - Issues, Methods and FAQ, World Weather Res. Program. Jt. Work. Gr. Verif., 2009. https://www.cawcr.gov.au/projects/verification/verif_web_page.html. (Accessed 1 December 2021).

[50] E. Ebert, Methods for verifying satellite precipitation estimates, in: V. Levizzani, P. Bauer, F.J. Turk (Eds.), Meas. Precip. From Sp. EURAINSAT Futur., Springer, Dordrecht, 2007, pp. 345–356, https://doi.org/10.1007/978-1-4020-5835-6_27.

[51] D.S. Wilks, Statistical Methods in the Atmospheric Sciences, third ed., Academic Press,Elsevier, 2011.

[52] J.E. Nash, J.V. Sutcliffe, River flow forecasting through conceptual models part I - A discussion of principles, J. Hydrol. 10 (1970) 282–290, https://doi.org/10.1016/0022-1694(70)90255-6.

[53] NCAR - Research Applications Laboratory, Verification: Weather Forecast Verification Utilities. R Package Version 1.42, 2015. https://cran.r-project.org/package=verification%0A.

[54] B. Hamner, M. Frasco, Metrics: Evaluation Metrics for Machine Learning. R Package Version, 2018, 0.1.4. https://cran.r-project.org/package=Metrics.

[55] J.E. Oliver, Monthly precipitation distribution : a comparative index, Prof. Geogr. 32 (1980) 300–309, https://doi.org/10.1111/j.0033-0124.1980.00300.x.

[56] M. De Luis, J.C. González-Hidalgo, M. Brunetti, L.A. Longares, Precipitation concentration changes in Spain 1946-2005, Nat. Hazards Earth Syst. Sci. 11 (2011) 1259–1265, https://doi.org/10.5194/nhess-11-1259-2011.

[57] A. Belay, T. Demissie, J.W. Recha, C. Oludhe, P.M. Osano, L.A. Olaka, D. Solomon, Z. Berhane, Analysis of climate variability and trends in Southern Ethiopia, Climate 9 (2021) 1–17, https://doi.org/10.3390/cli9060096.

[58] B.T. Kassie, R.P. Rötter, H. Hengsdijk, S. Asseng, M.K. Van Ittersum, H. Kahiluoto, D.H. Van Keulen, Climate variability and change in the Central Rift Valley of Ethiopia : challenges for rainfed crop production, J. Agric. Sci. 152 (2014) 58–74, https://doi.org/10.1017/S0021859612000986.

[59] A. Alemayehu, M. Maru, W. Bewket, M. Assen, Spatiotemporal variability and trends in rainfall and temperature in Alwero watershed, western Ethiopia, Environ. Syst. Res. 9 (2020) 1–15, https://doi.org/10.1186/s40068-020-00184-3.

[60] C.T. Agnew, A. Chappell, Drought in the sahel, Geojournal 48 (1999) 299–311, https://doi.org/10.1023/A:1007059403077.

[61] R. Mahmood, S. Jia, W. Zhu, Analysis of climate variability , trends , and prediction in the most active parts of the Lake Chad basin , Africa, Sci. Rep. 9 (2019) 1–18, https://doi.org/10.1038/s41598-019-42811-9.

[62] A. Panda, N. Sahu, Trend analysis of seasonal rainfall and temperature pattern in Kalahandi, Bolangir and Koraput districts of Odisha, India, Atmos. Sci. Lett. 20 (2019) 1–10, https://doi.org/10.1002/asl.932.

[63] H. von Storch, A. Navarra, Misuses of statistical analysis in climate research, in: H. von Storch, A. Navarra (Eds.), Anal. Clim. Var. Appl. Stat. Tech., Springer-Verlag, New York, 1995, pp. 11–26.

[64] P.K. Sen, Estimates of the regression coefficient based on kendall's tau, J. Am. Stat. Assoc. 63 (1968) 1379–1389, https://doi.org/10.1080/01621459.1968.10480934.

[65] M.G. Kendall, Rank Correlation Methods, 1948. San Francisco,CA.

[66] H.B. Mann, Non-parametric test against trend, Econometrica 13 (1945).

[67] R. R CoreTeam, A Language and Environment for Statistical Computing, R Foundation for Statistical Computing, Vienna, Austria, 2021.

[68] S. Yue, C.Y. Wang, The Mann-Kendall test modified by effective sample size to detect trend in serially correlated hydrological series, Water Resour. Manag. 18 (2004) 201–218, https://doi.org/10.1023/B:WARM.0000043140.61082.60.

[69] S.K. Patakamuri, N. O'Brien, Modifiedmk: Modified Versions of Mann Kendall and Spearman's Rho Trend Tests. R Package, 2021, version 1.6. https://cran.r-project.org/package=modifiedmk.

[70] M. Gocic, S. Trajkovic, Analysis of changes in meteorological variables using Mann-Kendall and Sen's slope estimator statistical tests in Serbia, Global Planet. Change 100 (2013) 172–182, https://doi.org/10.1016/j.gloplacha.2012.10.014.

[71] A. Baddeley, R. Turner, Spatstat: an R package for analyzing spatial point patterns, J. Stat. Software 12 (2005) 1–42, https://doi.org/10.18637/jss.v012.i06.

[72] A. Oztopal, Z. Sen, Innovative trend methodology applications to precipitation records in Turkey, Water Resour. Manag. 31 (2017) 727–737, https://doi.org/10.1007/s11269-016-1343-5.

[73] H. Wu, H. Qian, Innovative trend analysis of annual and seasonal rainfall and extreme values in Shaanxi, China, since the 1950s, Int. J. Climatol. 37 (2017) 2582–2592, https://doi.org/10.1002/joc.4866.

[74] A. Saini, N. Sahu, P. Kumar, S. Nayak, W. Duan, Advanced rainfall trend analysis of 117 Years over west coast plain and hill agro-climatic region of India, Atmosphere 11 (2020) 1–25, https://doi.org/10.3390/atmos11111225.

[75] S. Rosell, Regional perspective on rainfall change and variability in the central highlands of Ethiopia , 1978-2007, Appl. Geogr. 31 (2011) 329–338, https://doi.org/10.1016/j.apgeog.2010.07.005.

[76] T. Kifle, D.Y. Ayal, M. Mulugeta, Factors influencing farmers adoption of climate smart agriculture to respond climate variability in Siyadebrina Wayu District, Central highland of Ethiopia, Clim. Serv. 26 (2022) 1–10, https://doi.org/10.1016/j.cliser.2022.100290.

[77] A. Wassie, N. Pauline, Evaluating smallholder farmers ' preferences for climate smart agricultural practices in Tehuledere District , northeastern Ethiopia, Singap. J. Trop. Geogr. 39 (2018) 300–316, https://doi.org/10.1111/sjtg.12240.

[78] S. Rosell, B. Holmer, Rainfall change and its implications for belg harvest in South Wollo, Ethiopia, Geogr. Ann. Ser. A Phys. Geogr. 89 (2007) 287–299, https://doi.org/10.1111/j.1468-0459.2007.00327.x.

[79] Y. Mohammed, F. Yimer, M. Tadesse, K. Tesfaye, Variability and trends of rainfall extreme events in north east highlands of Ethiopia, Int. J. Hydrol. 2 (2018) 594–605, https://doi.org/10.15406/ijh.2018.02.00131.
[80] B.A. Miheretu, Temporal variability and trend analysis of temperature and rainfall in the Northern highlands of Ethiopia, Phys. Geogr. 42 (2021) 434–451, https://doi.org/10.1080/02723646.2020.1806674.
[81] W.B. Abegaz, E.A. Abera, Temperature and rainfall trends in north eastern Ethiopia, Int. J. Environ. Sci. Nat. Resour. 25 (2020) 97–103, https://doi.org/10.19080/IJESNR.2020.25.556163.
[82] A. Cherinet, Z. Mekonnen, Comparing farmers ' perception of climate change and variability with historical climate data : the case of ensaro district , Ethiopia, Int J Env. Sci Nat Res. 17 (2019) 114–120, https://doi.org/10.19080/IJESNR.2019.17.555966.